JOURNAL OF THE ROYAL SOCIETY Interface

Nested autoinhibitory feedbacks alter the resistance of homeostatic adaptive biochemical networks

Jörg Schaber, Anastasiya Lapytsko and Dietrich Flockerzi

J. R. Soc. Interface 2014 **11**, 20130971, published 4 December 2013

JOURNAL OF THE ROYAL SOCIETY Interface

rsif.royalsocietypublishing.org

Research

Cite this article: Schaber J, Lapytsko A, Flockerzi D. 2014 Nested autoinhibitory feedbacks alter the resistance of homeostatic adaptive biochemical networks. *J. R. Soc. Interface* **11**: 20130971.
http://dx.doi.org/10.1098/rsif.2013.0971

Received: 21 October 2013
Accepted: 12 November 2013

Subject Areas:
systems biology, computational biology, biomathematics

Keywords:
negative feedback control, Hopf bifurcation, high osmolarity glycerol, p53

Author for correspondence:
Jörg Schaber
e-mail: schaber@med.ovgu.de

Electronic supplementary material is available at http://dx.doi.org/10.1098/rsif.2013.0971 or via http://rsif.royalsocietypublishing.org.

Royal Society Publishing

Nested autoinhibitory feedbacks alter the resistance of homeostatic adaptive biochemical networks

Jörg Schaber[1], Anastasiya Lapytsko[1] and Dietrich Flockerzi[2]

[1]Institute for Experimental Internal Medicine, Medical Faculty, Otto von Guericke University, Magdeburg, Germany
[2]Max Planck Institute for Dynamics of Complex Technical Systems, Magdeburg, Germany

Negative feedback control is a ubiquitous feature of biochemical systems, as is time delay between a signal and its response. Negative feedback in conjunction with time delay can lead to oscillations. In a cellular context, it might be beneficial to mitigate oscillatory behaviour to avoid recurring stress situations. This can be achieved by increasing the distance between the parameters of the system and certain thresholds, beyond which oscillations occur. This distance has been termed resistance. Here, we prove that in a generic three-dimensional negative feedback system the resistance of the system is modified by nested autoinhibitory feedbacks. Our system features negative feedbacks through both input-inhibition as well as output-activation, a signalling component with mass conservation and perfect adaptation. We show that these features render the system applicable to biological data, exemplified by the high osmolarity glycerol system in yeast and the mammalian p53 system. Output-activation is better supported by data than input-inhibition and also shows distinguished properties with respect to the system's stimulus. Our general approach might be useful in designing synthetic systems in which oscillations can be tuned by synthetic autoinhibitory feedbacks.

1. Introduction

Negative feedback control is a fundamental and a ubiquitous feature of biochemical systems [1–6] and can mediate adaptation [7–10], stabilize the abundance of biochemical species [4,11,12], induce oscillations [3,5,13–16] and accelerate response times [11,17]. In fact, negative feedbacks have been observed in a wealth of biological systems ranging from mammalian cell cycle [13,18] to bacterial adaptation [8,19] and stress response in mammals [20] and yeast [21,22]. Another ubiquitous principle of biochemical systems is time delay between a signal and its response, which can, for example, be caused by the time needed to transcribe and translate biochemical information into cellular compounds. It is a long-standing theoretical result that negative feedbacks in conjunction with time delay can lead to stable oscillations [15,16,23]. Oscillatory behaviour brought about by delayed negative feedbacks has been observed and analysed in a range of biological systems, for example, the mammalian p53 system [24–26], and the NF-κB system [27–29]. Both the p53 as well as the NF-κB system mediate adaptation to external stimuli and stress, such as, for example, DNA damage. It is comprehensible that it might be beneficial to mitigate oscillatory behaviour during adaptation in order to avoid recurring stress situations. This can be achieved by moving the steady state of the system far away from certain thresholds, beyond which oscillations occur. The distance between such thresholds and the parameters of the system has been termed resilience and/or resistance. The larger the resistance of a system, the better perturbations in external or internal conditions, i.e. the systems parameters, can be absorbed, which otherwise would trigger a change in stability properties of the system [30,31]. There exist several

definitions of resistance in the literature [31]. Here, based on [31], we will refer to 'resistance' as the system's response to perturbations of parameter values. As a quantitative measure of resistance, we use the Euclidian distance of the parameter vector to a critical threshold, beyond which stability properties of the system change. The larger this distance, the more resistant is the system.

In a recent study, using a parametrized mathematical model, evidence was presented that during osmo-adaptation in yeast, which is largely mediated by a delayed negative integral feedback, the potential of oscillatory behaviour is reduced by introducing nested direct negative feedbacks [21]. Thus, there is evidence that in a concrete biological system nested negative feedbacks can increase the resistance of a biochemical network.

Here, using a generic three-dimensional model for integral negative feedback control of a biochemical network, we explore whether coupling autoinhibitory and delayed negative feedbacks might be a general cellular mechanism to increase resistance of a system. Our system has several distinguished features which generalize and extend former studies [15,16,32]:

— our models include components, which resemble post-translational modification of proteins conserving the total protein abundance (mass conservation), rendering the system more general and, at the same time, more realistic, especially with respect to signalling cascades;
— our models use integral feedback properties, i.e. some state variables of the system robustly track their desired values independent from the input [8], which also renders the systems more applicable to realistic situations, as shown below; and
— in our models, the delayed negative feedback may operate through both by inhibiting sensor inflow, like in [15], and by activating sensor outflow, like in [9]. This has been termed input and output control [10]. Here, we refer to these two control types as input-inhibition and output-activation, respectively. The type of used delayed negative feedback has important implications with respect to what actually stimulates the system. We show that an output-activation feedback mechanism is better supported by a range of data.

We prove that, in our systems, stable limit cycle oscillations can occur owing to a Hopf bifurcation. Further, we prove that the parameter region, where oscillations occur, can be reduced by introducing autoinhibitory feedbacks. Thus, by nesting autoinhibitory negative feedbacks into delayed negative feedbacks the structural stability of the system can be altered. This is true, in general, for input-inhibition systems. However, there exist certain limitations for this effect in output-activation systems. We also provide computational evidence that the sensitivity of the steady state with respect to parameter perturbations is decreased in system with nested autoinhibitory feedback. We apply our generic model to the high osmolarity glycerol (HOG) system in yeast, and the mammalian p53 system demonstrating the applicability of our general framework to concrete situations. We propose that this simple framework can be used to design synthetic systems in which oscillatory behaviour can be tuned by nesting direct, possibly autoinhibitory, and delayed negative feedbacks.

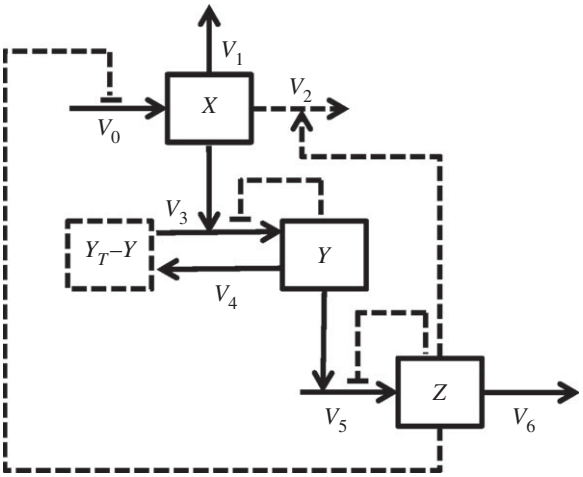

Figure 1. Wiring scheme of the generic integral feedback the model in (2.1). Dashed components indicate model alternatives, which were considered for concrete applications and the examples in the electronic supplementary material. Alternative kinetics are not indicated. Reaction numbers correspond to parameter numbers in (2.1). Specific wiring schemes can be found in the electronic supplementary material along with the respective examples.

2. Results

2.1. The model

In the following, we consider the three-dimensional system

$$\left.\begin{aligned} \frac{dx}{dt} &= k_0 q(z) - (k_1 x + k_2 f_1(x) f_3(z)), \\ \frac{dy}{dt} &= k_3 x (y_T - y) g(y, \kappa_y) - k_4 y \\ \text{and} \quad \frac{dz}{dt} &= k_5 y H(z, \kappa_z) - k_6 h(z). \end{aligned}\right\} \tag{2.1}$$

with positive parameters k_0, k_1, k_2, k_3, k_4, k_5, k_6, y_T, κ_y, κ_z and non-negative initial conditions x_0, y_0 and z_0. External perturbations are simulated by modifying the value of k_0 which otherwise mimics a basal stimulation of the system. This system can be even more generalized by replacing all linear functions x and y by smooth strictly increasing functions (see the electronic supplementary material). Figure 1 displays a wiring diagram of the system (2.1) also indicating different alternative model formulations that were tested in the application described below.

In general, $x(t)$ can be considered as a cellular sensor, which reacts to an external stimulus k_0. The component $y(t)$ mimics a signal transduction, which relays the input signal coming from the sensor $x(t)$ to the response component $z(t)$, which in turn negatively feeds back into the sensor $x(t)$ via $f_3(z)$ or via $q(z)$. We assume f_1,f_3, and h to be strictly increasing functions on $\mathbb{R}_{\geq 0}$ vanishing at 0. The function $q(z)$ is a smooth, positive and strictly decreasing function with $q(0) = 1$. The functions $f_3(z)$ and $q(z)$ represent the overall feedback in the system, respectively. In the examples below, we consider them to be mutually exclusive and refer to a feedback through $q(z)$ as input-inhibition, and a feedback through $f_3(z)$ as output-activation. The functions $g(y, \kappa_y)$ and $H(z, \kappa_z)$ are smooth, positive and decreasing in both arguments with $g(0, \kappa_y) = H(0, \kappa_z) = g(y, 0) = H(z, 0) = 1$. The functions $g(y, \kappa_y)$ and $H(z, \kappa_z)$ may represent autoinhibitory feedbacks, where we later consider the additional parameters κ_y and κ_z, which, among other parameters, shape the form of these

functions. We call them autoinhibitory, because the inhibition of a component depends only on itself and not on other system variables.

The term $(y_T - y)$ leads to a model with an *a priori* bound y for the second component in case its initial value $y(0)$ is in $[0, y_T]$. This term is obtained by reducing a four-dimensional $(x, y, \tilde{y}, z)$ system with $y_T = y + \tilde{y}$, mimicking a reversible post-translational modification, such as, for example, phosphorylation, of a protein y that does not affect the total protein abundance y_T (mass conservation).

Note that the non-negative orthant $\mathbb{R}^3_{\geq 0}$ is positive invariant for all models and, therefore, all models are biologically sound in the sense that no negative values for the components can occur. For further details, please refer to the electronic supplementary material.

Taken together, we analyse a generic model that comprises a range of special cases that have been addressed in the literature, for example, the Goodwin-type models [15,16,32], but also addresses models that have not been thoroughly analysed yet, especially the output-activation models, which will be shown to be especially relevant in concrete situations.

2.2. Integral feedback property

Integral feedback control is an engineering strategy that is supposed to ensure that the output of a system always adapts to its desired value independent of noise and of perturbations of the system parameters [8]. For two-dimensional systems, it has been reported that the kinetic nature of $h(z)$ is important in this respect; for example, mass action kinetics for $h(z)$ is not sufficient to obtain perfect adaptation for $y(t)$ [9,10]. For convenience of the mathematical analysis, we approximate a zero-order $h(z)$ by a smooth function $h : [0, \infty) \to [0, 1]$ with $h(0) = 0$, and $h(z) = 1$ for $z \geq a > 0$ and that is strictly increasing on $(0, a)$ and require that an equilibrium $\hat{z}$ exists with $\hat{z} > a$. Thus, $h(\hat{z}) = 1$ and, for $H \equiv 1$, the equilibrium of the second component

$$\hat{y} = \frac{k_6 h(\hat{z})}{k_5} = \frac{k_6}{k_5}$$

is constant and independent of the input signal in this limiting case.

Taken together, the system (2.1) approximates a perfect adaptor for zero-order $h(z)$ with respect to $y(t)$. Note that the above approximation is only a theoretical one ensuring that the solution stays in the positive orthant $\mathbb{R}^3_{\geq 0}$, unlike the approximation $K_z = 0$ for Michaelis–Menten type $h(z) = z/(K_z + z)$ for which negative solutions can occur. For concrete situations, it suffices to assume a sufficiently small K_z for the Michaelis–Menten type $h(z)$ implying $h(\hat{z}) \approx 1$.

2.3. The output-activation system is stimulated by the difference between the internal and external state

Zero-order kinetics for $f_1(x)$ has important implications with respect to what is actually sensed and integrated as error function by the system. Let us assume $q(z) \equiv 1$, a linear feedback function $f_3(z) = z$, and that the sensor $x(t)$ is in quasi-equilibrium with respect to the response variable z. Further, we approximate a zero-order $f_1(x)$, for example, $f_1(x) = x/(K_x + x)$, by a smooth function $f_1 : [0, \infty) \to [0, 1]$ with $f_1(0) = 0$, and $f_1(x) = 1$ for $x \geq a > 0$ and that is strictly increasing on $(0, a)$ and require that at the equilibrium $\hat{x} > a$. Thus, $f_1(\hat{x}) = 1$ and

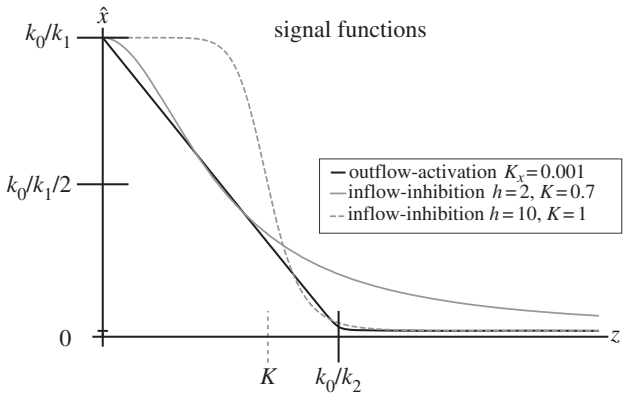

Figure 2. Signal functions, i.e. quasi-equilibrium sensor values $\hat{x}$ as a function of the response variable z for the system (2.1) with either $q(z) \equiv 1$ and $f_1(x)f_3(z) = xz/(K_x + x)$ (approximated by (2.2); black curve) or $k_2 = 0$ and $q(z) = 1/(1 + Kz^h)$ (2.4) (grey curves).

$$\hat{x} = \frac{k_0 - k_2 z}{k_1} > a \tag{2.2}$$

is a linear function of z. Thus, for zero-order $f_1(x) = x/(K_x + x)$ and linear output-activation, the system (2.1) is stimulated by the positive difference between the external stimulus k_0 and the scaled response variable z, i.e. the internal state. As above, this approximation is introduced for convenience of the theoretical analysis only. In real situations, it suffices to assume a sufficiently small K_x as in figure 2.

In the case of mass action kinetics for $f_1(x)$,

$$\hat{x} = \frac{k_0}{k_1 + k_2 z} \tag{2.3}$$

is related to the ratio between the external stimulus k_0 and the response variable z. A similar form for $\hat{x}$ as in (2.3) is obtained in a model with input-inhibition, i.e. $k_2 = 0$ and

$$q(z) = \frac{1}{1 + Kz^h},$$

which was assumed in the classical model of Goodwin [15,16,32]. Here, we obtain

$$\hat{x} = \frac{k_0}{k_1(1 + Kz^h)}. \tag{2.4}$$

In figure 2, we display quasi-equilibrium sensor values $\hat{x}$ as a function of the response variable z for the system (2.1) with either a Hill-type input-inhibition term as in [15] and $k_2 = 0$, or a zero-order output-activation term with linear feedback in z, i.e. $f_1(x)f_3(z) = xz/(K_x + x)$ with $q(z) \equiv 1$, respectively.

Note that in a system where the feedback is mediated through output-activation by a linear feedback with zero-order degradation, i.e. $f_1(x)\, f_3(z) = xz/(K_x + x)$ and $q(z) \equiv 1$, the response threshold k_0/k_2 is well defined for small K_x and can directly be tuned through k_2 (figure 2). Similarly, for systems with Hill-type input-inhibition, i.e. $k_2 = 0$ and $q(z) = 1/(1 + Kz^h)$, the response threshold is well defined for large Hill factors h (grey dashed line in figure 2), but can only indirectly be tuned through the half-saturation constant K. In addition, the better the threshold is defined by large Hill factors h, the sooner the sensor activation

saturates for decreasing z, whereas in a system with output-activation, sensor activation is linear below the activation threshold k_0/k_2. Conversely, when in a system with Hill-type input-inhibition, the sensor approximates a linear function in z (grey solid line in figure 2), the response threshold is poorly defined.

Taken together, the type (input-inhibition or output-activation) and kinetic nature (mass action or saturating) of the overall negative feedback determines the signal, which stimulates the system. In the case of zero-order output-activation, the system is linearly stimulated by the difference between internal and external conditions; otherwise, the stimulus is nonlinear and may even be step-like. In the examples below, we show that the data clearly support output-activation models rather than support nonlinear Goodwin-type input-inhibition models.

2.4. The Hopf bifurcation

In the system (2.1), stable limit cycles can occur due to a Hopf bifurcation. Shortly, any steady state $\hat{E} = (\hat{x}, \hat{y}, \hat{z})^T$ of the system (2.1) is given by

$$\hat{y} = Y(\hat{z}) := \frac{k_6 h(\hat{z})}{k_5 H(\hat{z}, \kappa_z)} < y_T, \quad \hat{x} = X(\hat{z}) := \frac{k_4 Y(\hat{z})}{k_3 G(Y(\hat{z}), \kappa_y)}. \tag{2.5}$$

We define $G(y, \kappa_y) = (y_t - y)g(y, \kappa_y)$ and the parameter value

$$\hat{k}_0 = P(\hat{z}, k_1) := \frac{1}{q(\hat{z})}(k_1 \hat{x} + k_2 f_1(\hat{x}) f_3(\hat{z})). \tag{2.6}$$

The Jacobian at the equilibrium $\hat{E} = (\hat{x}, \hat{y}, \hat{z})$ is of the form

$$J(E) = \begin{bmatrix} -A & 0 & -B \\ C & -D & 0 \\ 0 & E & -F \end{bmatrix} = \begin{bmatrix} -[k_1 + k_2 f_1'(\hat{x}) f_3(\hat{z})] & 0 & -[\hat{k}_0 |q'(\hat{z})| + k_2 f_1(\hat{x}) f_3'(\hat{z})] \\ k_3 G(\hat{y}, \kappa_y) & -[k_4 + k_3 \hat{x} |G'(\hat{y}, \kappa_y)|] & 0 \\ 0 & k_5 H(\hat{z}, \kappa_z) & -[k_5 \hat{y} |H'(\hat{z}, \kappa_z)| + k_6 h'(\hat{z})] \end{bmatrix}.$$

and has the characteristic Hurwitz-polynomial $\lambda^3 + \Delta_2 \lambda^2 + \Delta_1 \lambda^1 + \Delta_0$, with positive

$$\Delta_2 = A + D + F, \quad \Delta_1 = AD + AF + DF,$$
$$\Delta_0 = ADF + BCE.$$

So, any real eigenvalue of J is negative. The necessary and sufficient condition for a single pair $\pm i\omega = \pm i\sqrt{\Delta_1}$ $(\omega > 0)$ of pure imaginary eigenvalues is $\Delta_0 = \Delta_1 \Delta_2$, i.e.

$$BCE = (D + F)(A^2 + A(D + F) + DF). \tag{2.7}$$

evaluated at $\hat{E}$. With

$$A = k_1 + A_0, \quad A_0 := k_2 f_1'(X(\hat{z}, \kappa_y)) f_3(\hat{z})$$

$$B = k_1 B_1 + B_0, \; B_1 := X(\hat{z}, \kappa_y) \frac{|q'(\hat{z})|}{q(\hat{z})},$$

$$B_0 := k_2 f_1(X(\hat{z}, \kappa_y)) f_3(\hat{z}) \frac{|q'(\hat{z})|}{q(\hat{z})} + k_2 f_1(X(\hat{z}, \kappa_y)) f_3'(\hat{z}),$$

we consider (2.7) as an equation of the parameters k_1 and $\hat{z}$ that is to be solved in the form $k_1 = K_1(\hat{z})$. The curve $K_1(\hat{z})$, given by the unique positive solution $k_1 = K_1(\hat{z})$ of the quadratic equation, derived from (2.7),

$$k_1^2 + k_1 R_1(\hat{z}) - R_0(\hat{z}) = k_1^2 + k_1 \left(2A_0 + D + F - \frac{B_1 CE}{D + F}\right) + (A_0 + D)(A_0 + F) - \frac{B_0 CE}{D + F} = 0. \tag{2.8}$$

evaluated at $\hat{E}$, indicates possible Hopf-bifurcation points in the k_1-$\hat{z}$-plane. The necessary and sufficient condition of the existence for a positive k_1-solution of (2.8) is $R_0(\hat{z}) > 0$, i.e.

$$B_0 CE > (D + F)(A_0 + D)(A_0 + F). \tag{2.9}$$

Taken together, having chosen the equilibrium component $\hat{z}$, we define $\hat{x}$ and $\hat{y}$ according to (2.5), solve (2.8) for $k_1 = K_1(\hat{z}) > 0$, provided (2.9), and set $\hat{k}_0 = P(\hat{z}, k_1, \kappa_y)$ according to (2.6). Then, the possible Hopf-bifurcation point is given by $\hat{E} = (\hat{x}, \hat{y}, \hat{z})^T$ for the critical parameters k_1 and $\hat{k}_0$.

In this case, the transversality condition for a Hopf bifurcation can be generically fulfilled (see the electronic supplementary material, where also further details of the proof are supplied). Thus, the system (2.1) can show stable oscillations owing to a Hopf bifurcation.

A Hopf bifurcation can also occur for a more general class of systems, where all linear functions x and y in the system (2.1) are replaced by smooth strictly increasing functions and with or without the term $(y_T - y)$ (see the electronic supplementary material).

2.5. Autoinhibition decreases the oscillatory k_1-$\hat{z}$-plane

In the electronic supplementary material, we prove that the k_1-$\hat{z}$-plane permissive for oscillations decreases with increasing autoinhibition either through $g(y, \kappa_y)$ or $H(z, \kappa_z)$, i.e. for the curve $K_1(\hat{z})$ that divides the k_1-$\hat{z}$-plane into regions with and without stable oscillations it holds

$$\frac{dK_1(\hat{z}, \kappa_y)}{d\kappa_y} < 0 \quad \text{and} \quad \frac{dK_1(\hat{z}, \kappa_z)}{d\kappa_z} < 0 \quad \forall \hat{z} > 0. \tag{2.10}$$

Again, there is a notable difference between models with input-inhibition, i.e. $k_2 = 0$, and output-activation, i.e. $q(z) \equiv 1$.

For models with input-inhibition relation, (2.10) is always true. This has been shown before for the classical Goodwin-type models with Hill-type q, i.e. $q(z) = 1/(1 + Kz^h)$ [32]. However, opposed to these classical models, where a high Hill coefficient (cooperativity) of $h \geq 8$ was necessary to obtain oscillations, this is not necessary in our framework (2.1) (see the electronic supplementary material, figures S4 and S7).

For models with output-activation condition (2.10) only applies, if $f_1(\hat{x}) = 1$, i.e. if at the equilibrium f_1 is of zero-order such that $f_1'(\hat{x}) = 0$. This situation can be approximated, e.g. by low K_x values for $f_1(x) = x/(K_x + x)$. Note that this was also a prerequisite for the quasi-steady state $\hat{x}$ to be a linear function of z as in (2.2). However, to reduce the parameter region for oscillations for the output-activation system, $f_1'(\hat{x}) = 0$ is sufficient, but not necessary (for examples, refer to the electronic supplementary material).

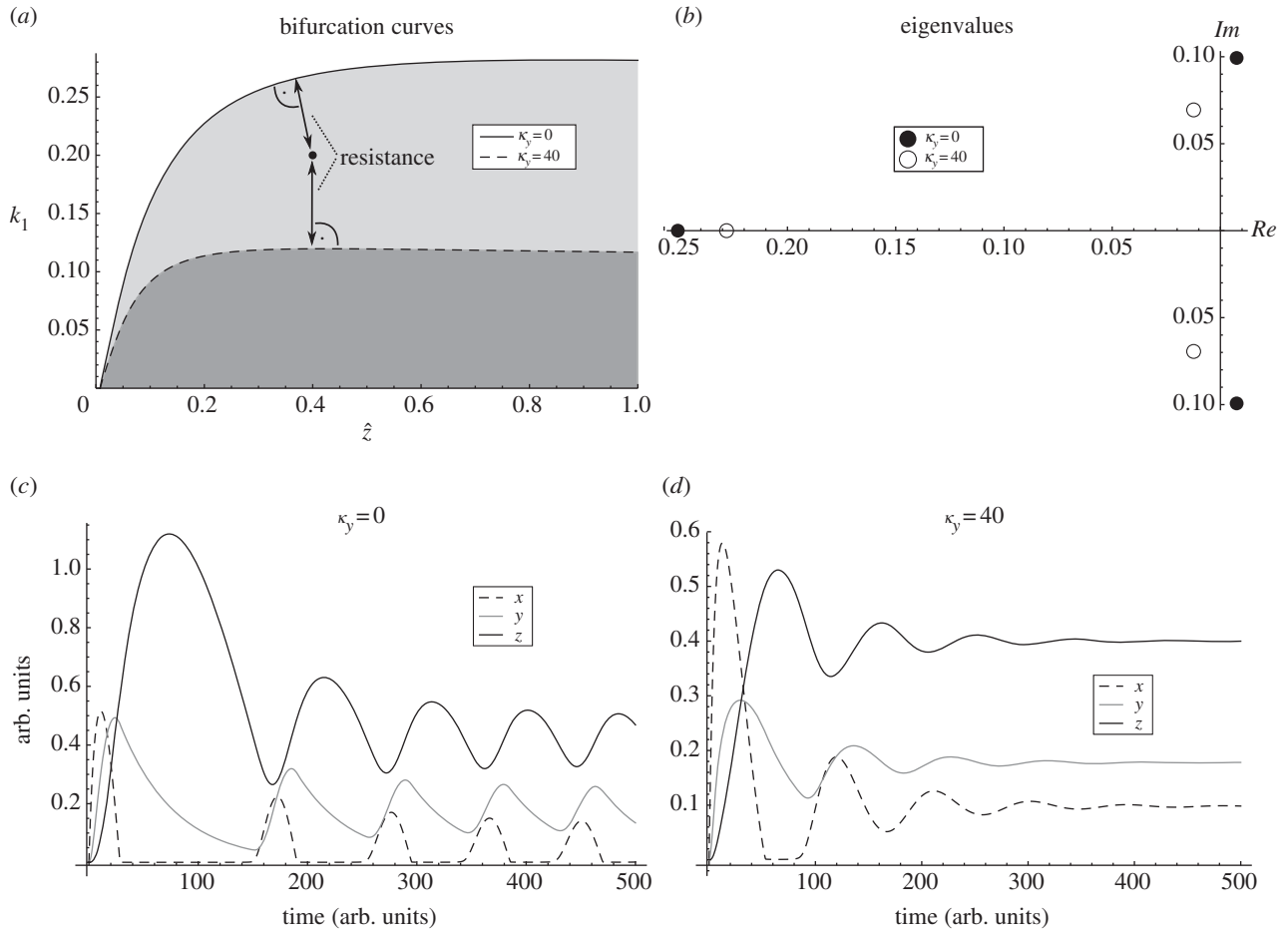

Figure 3. Bifurcation curves, eigenvalues and dynamics for the system (2.1) with $q(z) \equiv 1$, $f_1(x) = x/(K_x + x)$, $f_3(z) = z$, $g(y, \kappa_y) = 1/(1 + \kappa_y y^m)$ and $H(z) \equiv 1$, $h(z) = z/(K_z + z)$. (*a*) Bifurcation curves in k_1-$\hat{z}$-plane for $\kappa_y = 0$ and $\kappa_y = 40$, respectively. The distance between the parameters of the system, in this case $(\hat{z}, k_1)$, and the bifurcation threshold, i.e. $K_1(\hat{z})$, can be interpreted as a measure for resistance. (*b*) Eigenvalues of the Jacobian of the system (2.1) for $\kappa_y = 0$ and $\kappa_y = 40$, respectively. (*c*) Simulations for $(\hat{z}, k_1) = (0.4, 0.2)$ and $\kappa_y = 0$. (*d*) Simulations for $(z_0, k_1) = (0.4, 0.2)$ and $\kappa_y = 40$. Other parameters: $k_2 = 0.3$, $k_3 = k_5 = 0.1$, $k_4 = k_6 = 0.02$, $K_x = 0.0001$, $K_z = 0.05$, $m = 2$.

Taken together, we provide formal proof that the structural stability of the system (2.1) can be altered by introducing autoinhibitory feedbacks. Moreover, the distance between the bifurcation threshold and a given k_1-$\hat{z}$ pair can be modulated by introducing autoinhibitory negative feedbacks. Thus, nested autoinhibitory feedbacks can modulate the resistance of the system (2.1). Figure 3 illustrates these theoretical results for an output-activation system. For other examples, please refer to the electronic supplementary material, figures S2–S7.

In figure 3*a*, we show bifurcation curves in the k_1-$\hat{z}$-plane, for different values of κ_y, i.e. with ($\kappa_y = 40$) or without ($\kappa_y = 0$) autoinhibitory feedback for a concrete system. The area below the curve, where oscillations occur, is reduced with κ_y increasing. The larger κ_y, i.e. the stronger the autoinhibitory feedback, the smaller the area below the curve. The dot in figure 3*a* indicates a concrete pair of k_1-$\hat{z}$, to which the computed eigenvalues in figure 3*b* and dynamics in figure 2*c*,*d* correspond. The distance between a point in the k_1-$\hat{z}$ and the bifurcation curve $K_1(\hat{z})$ can be interpreted as a measure for resistance. Note that a change in $\hat{z}$ can also be interpreted as a change in parameter $\hat{k}_0$, because there is a 1 : 1 relationship between $\hat{z}$ and $\hat{k}_0$ (see (2.6)). Without autoinhibitory feedback ($\kappa_y = 0$), the bifurcation parameters are below the bifurcation curve and, consequently, we have a single pair of complex eigenvalues with positive real parts (black dots in figure 3*b*) corresponding to stable oscillations (figure 3*c*). With autoinhibitory feedback ($\kappa_y = 40$), the bifurcation parameters are above the bifurcation curve and, consequently, all real parts of the eigenvalues are negative (circles in figure 4*b*), and the system tends to a stable equilibrium (figure 3*d*).

For convenience, we conducted the theoretical analysis by parametrizing the system with respect to the steady state in $\hat{z}$ and considered k_1 as the bifurcation parameter. However, as illustrated by the computational analysis of the HOG system and the p53 system below, all tested parameters in the system may be taken as bifurcation parameters (figures 4 and 7; electronic supplementary material, S9 and S10). Accordingly, the introduction of autoinhibitory feedbacks reduces the region for oscillations for those parameters as well.

2.6. Application to the high osmolarity glycerol system

The HOG system in yeast mediates adaptation to a hyperosmotic shock and is one of the best-studied eukaryotic signalling pathways [33]. Several mathematical models of different complexity have been developed for this system [21,22,34,35]. In short, the signal that triggers response, and adaptation is supposedly related to volume [36,37], which, in turn, is proportional to the difference between internal and external osmotic pressure [38]. The signal coming from the membrane is transduced via a stress-activated protein kinase (SAPK) cascade, which culminates in the activation the SAPK Hog1. Hog1 translocates to the nucleus-activating transcription factors that lead to the upregulation of glycerol production,

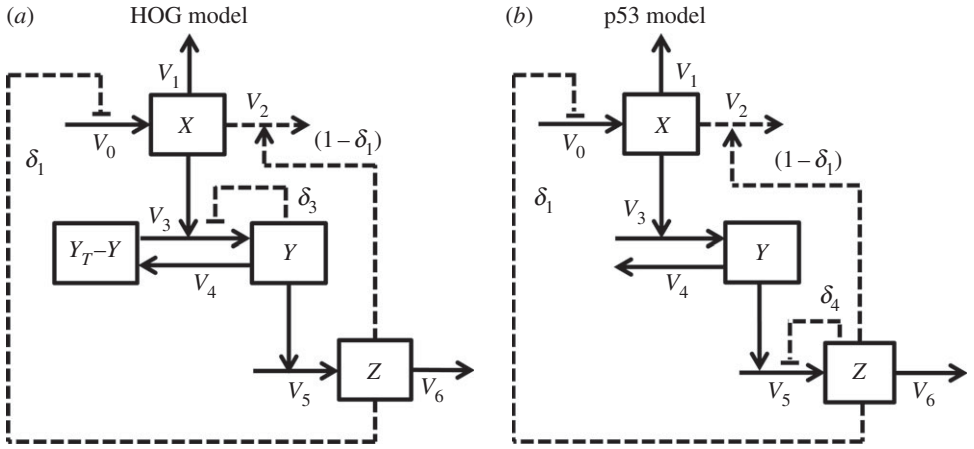

Figure 4. Subset of model alternatives from the system (2.1) (figure 1) tested for the HOG (2.11) and the p53 system (2.12). (*a*) Wiring schemes of the HOG system. Dashed components indicate the considered model alternatives that correspond to the indicated δ-values in (2.11). (*b*) Wiring schemes of the p53 system. Dashed components indicate the considered model alternatives that correspond to the indicated δ-values in (2.12). Components names are adapted for the concrete system. Alternative kinetics are not indicated. Reaction numbers correspond to parameter numbers in the system (2.1).

Table 1. HOG candidate models. *n*, number of data points; *k*, number of parameters; SSR, weighted sum of squared residuals; AIC*c*, Akaike information criterion corrected for small sample size; AIC*w*, Akaike weights.

rank	model no.	δ	*n*	*k*	SSR	AICc	AICw
1	6	(0,1,1,0)	67	8	7.5	61.5	0.8
2	8	(0,1,1,1)	67	9	7.5	64.4	0.2
3	2	(0,1,0,0)	67	6	15.3	104.6	0
4	4	(0,1,0,0)	67	7	15.3	107.2	0
5	11	(1,0,1,0)	67	8	16.3	113.9	0
6	9	(1,0,0,0)	67	6	44.3	175.9	0
7	10	(1,0,0,1)	67	7	44.7	179.0	0
8	12	(1,0,1,1)	67	9	44.7	184.2	0
9	1	(0,0,0,0)	67	5	52.0	184.1	0
10	3	(0,0,0,1)	67	6	53.2	188.1	0
11	5	(0,0,1,0)	67	7	52.0	189.1	0
12	7	(0,0,1,1)	67	8	53.2	193.2	0

which, in turn, increases the intracellular osmolarity and turgor, thereby mediating adaptation. There is evidence that in this system oscillatory behaviour might indeed be avoided by nested negative feedbacks [21]. Therefore, we tested whether our general framework is supported by available data, and, whether the data support autoinhibitory feedbacks. We fitted different candidate models representing different hypothesis about the underlying biochemical mechanisms and ranked them according to the Akaike information criterion (AIC). The candidate models were specified versions of our general framework (2.1) (figure 4*a*):

$$\left.\begin{aligned}\frac{\mathrm{d}x}{\mathrm{d}t} &= \frac{k_0+\mathrm{NaCl}}{(1+Kz^h)^{\delta_1}} - \left(k_1x + (1-\delta_1)k_2\frac{xz}{(K_x+x)^{\delta_2}}\right),\\ \frac{\mathrm{d}y}{\mathrm{d}t} &= k_3x\frac{(y_T-y)}{(1+\kappa_y y^m)^{\delta_3}} - k_4y\\ \text{and}\quad \frac{\mathrm{d}z}{\mathrm{d}t} &= k_5y - k_6\frac{z}{(K_z+z)^{\delta_4}},\end{aligned}\right\} \tag{2.11}$$

where $\delta=(\delta_1,\delta_2,\delta_3,\delta_4)$ and $\delta_i\in\{0,1\}$, $i=1,\ldots,4$ indicate model alternatives. Here, x represents a putative sensor of volume change or the difference between internal and external water potentials, i.e. z and $k_0+\mathrm{NaCl}$, respectively. The component y represents the adaptive phosphorylated Hog1 and z represents the integrator glycerol (figure 4*a*). Specifically, we tested the kind of delayed feedback, i.e. input-inhibition ($\delta_1=1$) or output-activation ($\delta_1=0$), the existence of autoinhibition in the signalling component y (δ_3) and two different kinetics for $f_1(x)$ and $h(z)$, respectively, i.e. mass action (δ_2, $\delta_4=0$) or Michaelis–Menten kinetics (δ_2, $\delta_4=1$). The combination of all these model alternatives yielded 12 different models. Here, we assumed $f_3(z)=z$ and $H(z,\kappa_z)\equiv 1$. For parameters of the best-ranked model, please refer to the electronic supplementary material, table S2. For more details on the model and parameter estimation, please refer to the Methods section and the electronic supplementary material. A COPASI implementation of the best-ranked model together with the data and an systems biology mark-up language (SBML) [39] version is also provided in the electronic supplementary material. The results of fitting and ranking are displayed in table 1.

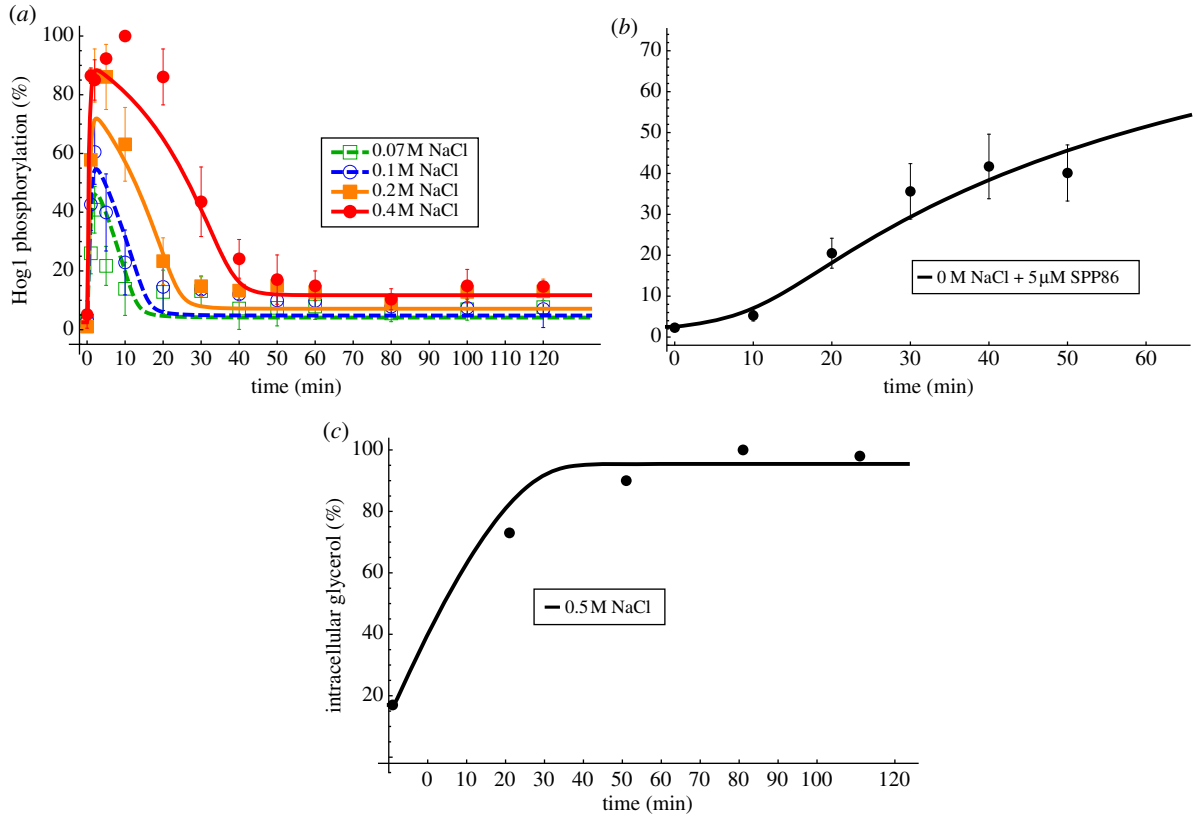

Figure 5. HOG system. Data and fit for the best approximating model no. 6, $\delta = (0, 1, 1, 0)$. (*a*) Measured (symbols, mean $\pm$ s.d. ($n \geq 3$) from [17]) and simulated (lines) phosphorylated Hog1 (y) for different osmotic stress conditions. (*b*) Measured (symbols) and simulated (lines) phosphorylated Hog1 (y) in experiments without osmotic shock and where Hog1 kinase activity was inhibited by the kinase inhibitor SPP86. (*c*) Measured (symbols) and simulated (lines) glycerol (z) upon an osmotic shock of 0.5 M NaCl. For the source of the experimental data, please refer to section Materials and methods. (Online version in colour.)

The model with zero-order kinetics in $f_1(x)$, autoinhibition in y and mass action kinetics in $h(z)$ is ranked best (model no. 6, $\delta = (0, 1, 1, 0)$). This corresponds to a model, which senses the difference between external and internal osmolarity and shows no perfect adaptation. This model is closely followed by the same model, but with perfect adaptation (model no. 8, $\delta = (0, 1, 1, 1)$). The best model without autoinhibition in y is on the third place (model no. 2, $\delta = (0, 1, 0, 0)$). The best two models are able to recapitulate Hog1 phosphorylation and intracellular glycerol data for a range of different conditions (figure 5). Model no. 2 can also well recapitulate Hog1 osmotic stress and glycerol data, but cannot recapitulate well the Hog1 inhibition experiment (see electronic supplementary material, figure S8). The models with an input-inhibition did not give a good approximation to the data compared with the best-ranking models (table 1).

Apparently, both the system with and without autoinhibitory feedback can show adaptive behaviour. Analysing the stability of the steady state as a function of the parameters, it becomes obvious that the parameter region, where oscillations occur, is much more distant from the actually fitted parameters for the model with (model no. 6) than for the model without autoinhibition (model no. 2). Thus, the resistance of the adaptation is increased in the system including the autoinhibitory feedback. Perturbing the initial steady state, which was also set in this case, had no influence on the stability, i.e. the system is resistant with respect to a change in initial steady-state concentrations (see the electronic supplementary material, figure S9). In figure 6, we plot the stability regions of the steady state in the two-dimensional k_5-NaCl and k_5-k_1 plane. For other parameter combinations, please refer to the electronic supplementary material, figure S9. Notably, the parameters of both the system with autoinhibition (model no. 6) and the system without autoinhibition (model no. 2) are rather similar (black and grey dots in figure 6 and the electronic supplementary material, S9). This indicates that the stability of a system can be modified by changing the system's structure by autoinhibition without significantly affecting other system parameters and, therefore, its dynamics (figure 5 and the electronic supplementary material, S8).

It can be anticipated that in homeostatic adaptive systems the steady state should be robust against parameter perturbations. It has been shown that negative feedbacks can increase the robustness of the steady states with respect to input noise and parameter perturbations [4,11,12]. We hypothesized that nested autoinhibitory feedbacks can increase the robustness of the steady state. Therefore, we compared the steady-state variability with respect to parameter perturbation of the best model with feedback (model no. 6) and the best model without feedback (model no. 2) after an osmotic shock of 0.2 M NaCl in a Monte Carlo analysis. Specifically, we perturbed all free parameters of the system simultaneously by sampling 1000 times from a uniform distribution ranging from half to double of its original value. Subsequently, we calculated the distance between the original fitted steady state and the perturbed steady states (figure 7).

The variance of the distance between the original and the perturbed steady states of the sensor x is significantly smaller ($p < 0.01$) for the model with autoinhibitory feedback (model no. 6) compared with the model without autoinhibitory feedback (model no. 2; figure 7). In addition, the respective variance for components y is smaller ($p < 0.01$; the electronic supplementary material, table S1). For the response z, no significant difference was detected. Thus, in

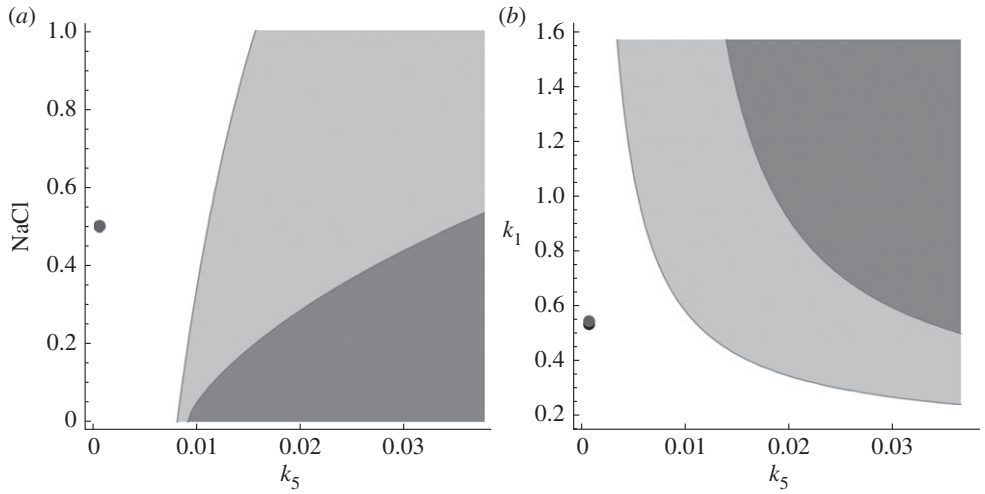

Figure 6. Stability region plots for the HOG system. (*a*,*b*) Shows stability regions for different parameter combinations. In (*a*,*b*), dark grey and light grey indicate regions with unstable steady state, i.e. where oscillations occur, for the system with (model no. 6) and without autoinhibitory feedback (model no. 2), respectively. Black and dark grey dots indicate the fitted parameters for the system with (model no. 6) and without autoinhibitory feedback (model no. 2), respectively. The boundary between white and shaded regions indicates bifurcation lines in the respective two-dimensional parameter space. For more stability region plots for different parameter combinations, please refer to the electronic supplementary material.

this concrete case, the autoinhibitory feedback increases robustness of the steady states after osmotic shock for the sensor and activated Hog1.

Taken together, our three-dimensional framework is able to recapitulate well a range of data for different conditions for the HOG system. Model discrimination suggests that in the HOG system there are autoinhibitory feedbacks nested within the glycerol-mediated feedback, and the system is stimulated by the difference between internal and external conditions. This is well supported by other studies [17,21]. Moreover, the autoinhibitory feedback renders the steady state of the system more resistant in the sense that parameter perturbations and external stress conditions are unlikely to drive the system beyond the threshold where oscillations occur.

2.7. Application to the p53 system

The p53 system is one of the best-studied human signalling pathways, which is activated by various stress signals, including DNA damage [40,41]. Interestingly, p53 phosphorylation can exhibit both oscillatory behaviour and sustained activation, depending on the stimulus, which imply different cell fates [26,42]. A range of models have been developed for this pathway to understand dynamics and variability of the protein circuitry [24,25,43]. Here, we tested whether our modelling framework can also explain p53 and Mdm2 dynamics, possibly giving new insights into the feedback regulation circuitry of the system. To this end, we fitted again different model alternatives based on our general framework (2.1) to a published average oscillation pattern of p53 and Mdm2 dynamics after DNA damage [25] (figure 4*b*):

$$\left.\begin{aligned}\frac{dx}{dt}&=\frac{k_0}{(1+Kz^h)^{\delta_1}}-\left(k_1x+(1-\delta_1)k_2\frac{x}{(K_x+x)^{\delta_2}}\frac{z^{n\delta_3}}{(K_1^n+z^n)^{\delta_3}}\right),\\ \frac{dy}{dt}&=k_3x-k_4y\\ \text{and }\frac{dz}{dt}&=k_5y\frac{1}{(1+\kappa_z z^m)^{\delta_4}}-k_6\frac{z}{(K_z+z)^{\delta_5}},\end{aligned}\right\}\tag{2.12}$$

where $\delta=(\delta_1,\delta_2,\delta_3,\delta_4,\delta_5)$, $\delta_i\in\{0,1\}$, $i=1,\ldots,5$, indicate model alternatives. Now, our model components are interpreted such that the signal x is p53 activation (sensing e.g. DNA damage), and the transducer y is an intermediate component, e.g. Mdm2 RNA. Consequently, for the latter component, no mass conservation is assumed, i.e. without the term (y_t-y) in (2.1). The response z represents Mdm2 protein concentration which, in turn, mediates p53 degradation. Like for the HOG model, we tested two kinetic alternatives for reactions $f_1(x)$, and $h(z)$, i.e. mass action (δ_2, $\delta_5=0$) or Michaelis–Menten kinetics (δ_2, $\delta_5=1$). In the p53 models, we assumed $g(y,\kappa_y)\equiv 1$, because, assuming the transducer to be RNA, a fast autoinhibitory feedback seemed unlikely. Therefore, we tested autoinhibition in component z by alternatively introducing $H(z,\kappa_z)=1/(1+\kappa_z z^m)$ (δ_4), assuming the fast autoinhibitory feedback to act at the protein level by, e.g. post-translational modifications. The kinetic nature of the negative feedback of Mdm2 on p53 remains elusive. Therefore, we also tested here two different alternatives for $f_3(z)$, i.e. mass action ($\delta_3=0$) and Hill-type kinetics ($\delta_3=1$). Additionally, we tested, as for the HOG system, the possibility that the negative feedback acts by input-inhibition ($\delta_1=1$) or by output-activation ($\delta_1=0$). Combination of the different possibilities results in 20 different models. The result of the fitting and ranking is displayed in table 2. For parameters of the best-ranked model, please refer to the electronic supplementary material, table S3. A COPASI implementation of the best-ranked model together with the data and an SBML version is also provided in the electronic supplementary material.

The two best-ranked models (no. 11, $\delta=(0,0,1,0,1)$ and no. 15, $\delta=(0,0,1,1,1)$) feature mass action kinetics in $f_1(x)$, Hill-type kinetics in $f_3(z)$, and zero-order kinetics in $h(z)$ and their fit is significantly better than for the other model candidates. Whether or not these two models have an autoinhibitory feedback does not influence the goodness fit itself (sum of squared residual (SSR) in table 2), but as the model without autoinhibitory feedback has two parameters less, it is clearly ranked first. The fit of the best approximating model no. 11 is shown in figure 8.

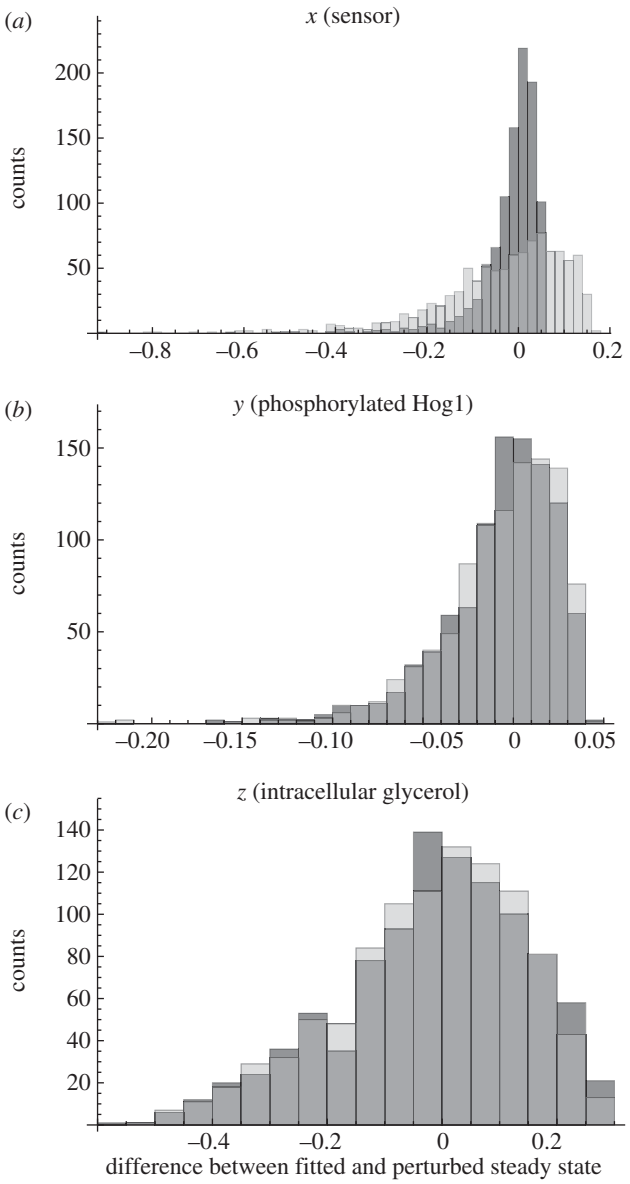

Figure 7. Monte Carlo analysis of the best approximating model with and without autoinhibitory feedback of the HOG system. (*a–c*) Shows the distributions of the difference between the original and the perturbed calculated steady states of the model with autoinhibitory feedback no. 6 (dark grey) and the model without autoinhibitory feedback no. 2 (light grey), respectively, for one of the three model components as indicated in the respective panel title. The dark grey regions indicate overlapping distributions. The free parameters (see electronic supplementary material, table S1) were perturbed by sampling 1000 times from a uniform distribution ranging from half to double of their original values and calculating the according steady states after an osmotic shock on 0.2 M NaCl.

The p53 system can show both oscillatory as well as sustained behaviour, depending on the stimulus [26,42]. Therefore, we asked the question whether the oscillations of the best approximating model can be stabilized by introducing a fast autoinhibitory feedback. This is only true in general, i.e. irrespective of the other parameters, when $f_1(x)$ has zero-order kinetics at the equilibrium, which is not the case for the best approximating p53 model no. 11. However, with the given set of parameters, our fitted model can indeed be stabilized by the introduction of an autoinhibitory feedback of the form $H(z, \kappa_z) = 1/(1 + \kappa_z z^m)$, with $\kappa_z = 1.95$ and $m = 3$ (figure 9).

Figure 9 depicts the stability of the steady state of the best approximating model with and without autoinhibitory feedback as a function of selected parameters (for additional pairs of parameters, refer to the electronic supplementary material, figure S10). Like for the HOG model, the unstable region diminishes through the introduction of a nested autoinhibitory feedback. Moreover, the stability of the system changes upon addition of the nested autoinhibitory feedback, rendering the system in the stable zone after introduction of an autoinhibitory feedback.

For the p53 system, a Monte Carlo analysis of the steady state with respect to parameter perturbations also indicated that the system with autoinhibitory feedback is less sensitive (figure 10).

The variance of the distance between the original and the perturbed steady states for all steady states is significantly smaller ($p < 0.001$) for the model with autoinhibitory feedback (model no. 15) compared with the model without autoinhibitory feedback (model no. 11; figure 10 and the electronic supplementary material, table S4).

Taken together, our simple framework suggests a mechanism how the p53 signalling system can change its dynamic behaviour upon different stimuli. Certain stimuli might activate components which introduce a nested autoinhibitory feedback. This changes the stability landscape of the system, shifting it from an oscillatory regime into a stable one. Thus, the p53 system depicts low resistance to parameter perturbations in order to be able to change its stability properties depending on environmental conditions.

3. Discussion

The ability to adapt to perturbations in external or internal conditions without losing structural stability is a fundamental feature of biological systems, including ecological, climate or biochemical systems. Adaptation is often mediated by negative feedbacks [1,7]. In biochemical systems, negative feedbacks inevitably come with time delays, which may lead to oscillatory behaviour both damped and sustained [15,23]. In some instances, oscillatory behaviour might oppose efficient adaptation owing to recurring stress. In such cases, the distance between the state of a system and the threshold beyond which oscillations occur, i.e. the systems resistance, should be large. This way, perturbations can be absorbed without affecting the structural stability of the system. In other instances, however, it might be beneficial to be able to switch between different dynamic regimes. It has been shown that the difference between a sustained or oscillatory signal can control cell fate [26,44], and that oscillation frequency can encode biochemical information [45]. In that case, resistance of a system should be low to be able to easily shift between different stability regimes. It might also be desirable to synthetically engineer cellular systems in a way such that oscillatory behaviour can be tuned by an independent artificial component.

For a three-dimensional system, it has been observed that coupling autoinhibitory and delayed negative feedbacks reduces the probability of occurrence of stable limit cycles [5]. For the simple gene transcription network model with input-inhibition proposed by Goodwin [15], it has been shown that nested self-repressing feedback loops have the potential to suppress oscillations [32]. Here, we propose a generic mechanism,

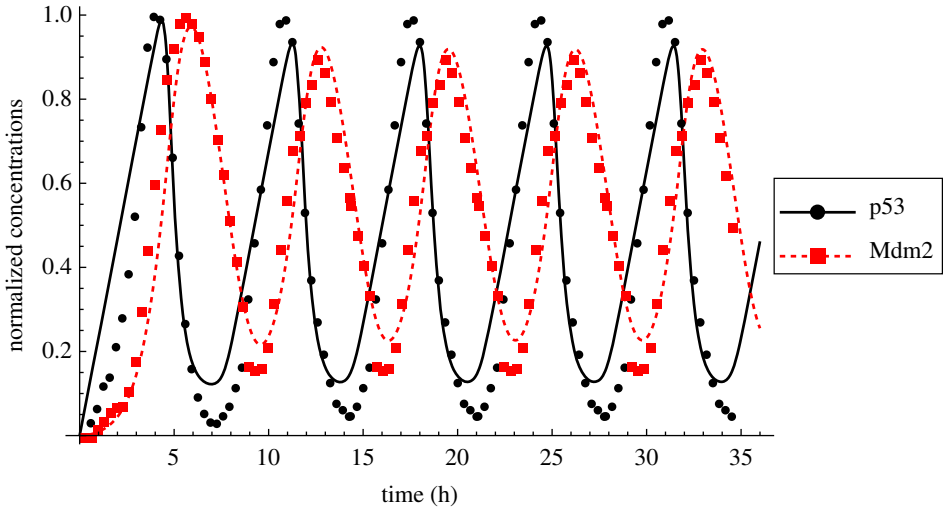

Figure 8. Data (adapted from [25]) and fit of the best approximating p53 model no. 11, $\delta = (0, 0, 1, 0, 1)$. Measured (symbols) and simulated (lines) concentrations for p53 (x, black, solid) and Mdm2 (z, red, dashed). For the source of the experimental data, please refer to section Materials and methods. (Online version in colour.)

Table 2. p53 candidate models. n, number of data points, k, number of parameters; SSR, weighted sum of squared residuals; AICc, Akaike information criterion corrected for small sample size; AICw, Akaike weights.

rank	model	δ	n	k	SSR	AICc	AICw
1	11	(0,0,1,0,1)	91	10	1.8	−76.8	1.0
2	15	(0,0,1,1,1)	91	12	1.8	−68.8	0.02
3	16	(0,1,1,1,1)	91	13	2.8	−26.4	0
4	10	(0,1,1,0,0)	91	10	2.9	−31.1	0
5	14	(0,1,1,1,0)	91	12	3.0	−25.6	0
6	7	(0,0,0,1,1)	91	10	4.5	7.3	0
7	3	(0,0,0,0,1)	91	8	5.0	12.2	0
8	4	(0,1,0,0,1)	91	9	5.0	14.2	0
9	8	(0,1,0,1,1)	91	11	5.1	20.7	0
10	9	(0,0,1,0,0)	91	9	5.6	25.1	0
11	13	(0,0,1,1,0)	91	11	5.6	30.3	0
12	18	(1,0,0,0,0)	91	9	10.5	81.8	0
13	20	(1,0,0,1,1)	91	11	11.0	91.6	0
14	17	(1,0,0,0,0)	91	8	12.0	91.6	0
15	6	(0,1,0,1,0)	91	10	12.4	99.9	0
16	2	(0,1,0,0,0)	91	8	13.3	101.0	0
17	19	(1,0,0,1,0)	91	10	16.1	123.1	0
18	1	(0,0,0,0,0)	91	7	16.7	119.1	0
19	5	(0,0,0,1,0)	91	9	16.7	124.0	0
20	12	(0,1,1,0,1)	91	11	18.1	136.7	0

how adaptive homeostatic biochemical systems can control both its dynamic response and its distance to a threshold beyond which these dynamics are drastically altered. We provide complete proof that in generic three-dimensional homeostatic adaptive biochemical networks both with input-inhibition as well as with output-activation oscillations may arise due to a Hopf bifurcation. We further prove that nested autoinhibitory feedbacks diminish the parameter space in which the steady state becomes unstable and oscillations occur. For systems with input-inhibition, the region for oscillations is generally reduced by autoinhibitory feedbacks. This is also true for models with a signalling module (mass conservation) and perfect adaptation (zero-order $h(z)$). The latter renders input-inhibition systems susceptible to oscillations also for low cooperativity in the input-inhibition which extends former studies [16,32,46]. For our system with output-activation, this is only true irrespective of the parameters, when the feedback-activated output is of zero-order. Thus, this is a sufficient, but not necessary condition. We show that this condition also has as the consequence that

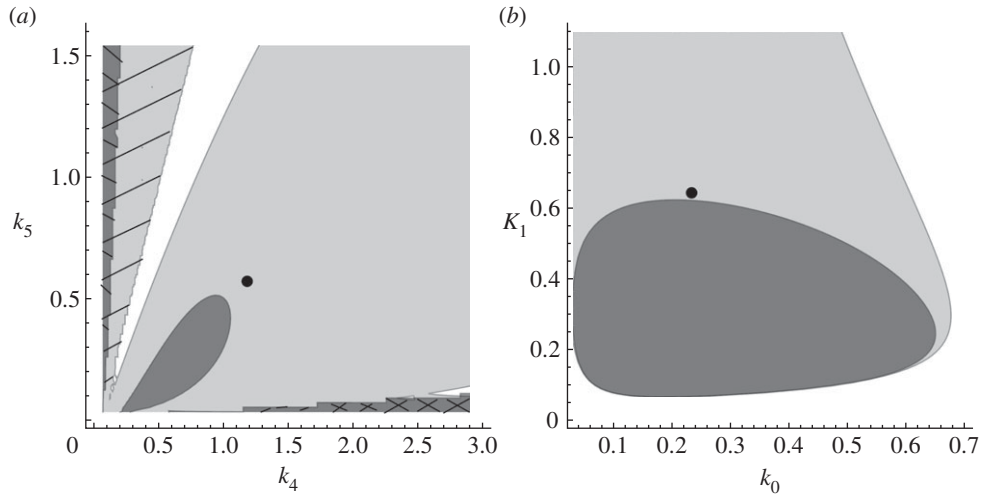

Figure 9. Stability region plots for the best approximating p53 model (model no. 11). (*a*,*b*) Shows stability regions for different parameter combinations. In (*a*,*b*), dark grey and light grey indicate regions with unstable steady state, i.e. where oscillations occur, for the system with a feedback of the form $H(z, \kappa_z) = 1/(1 + \kappa_z z^m)$ ($\kappa_z = 1.95$ and $m = 3$), and without autoinhibitory feedback, respectively. Black dots indicate the fitted parameters for the best approximating p53 model (model no. 11). The hatched regions indicate parameter combinations without steady state. The boundary between white and shaded regions indicates bifurcation lines in the respective two-dimensional parameter space. For more stability region plots for different parameter combinations, please refer to the electronic supplementary material.

the system is stimulated by the positive difference between external and internal conditions. Our applications to the HOG and the p53 system suggest that zero-order output-activation might be a biologically more relevant feedback mechanism than input-inhibition. For the adaptive HOG system, we also demonstrate that a nested autoinhibitory feedback can alter the structural stability of the system without significantly affecting parameters of the system that are not involved in this feedback. Therefore, autoinhibition can alter stability properties of a system without affecting dynamic properties within a certain range of conditions. Owing to the generality of our model, we may hypothesize that other kinds of nested feedbacks also have the potential to suppress oscillatory behaviour. Here, we analysed only autoinhibitory feedback for mathematical convenience. However, in the special case of a Goodwin-type model, it has been shown that a nested feedback from z to y also diminishes the parameter region in which oscillations occur [32]. In addition, for a four-dimensional model, it has even been demonstrated that a feedforward loop within an integral negative feedback also diminishes the parameter regions in which oscillations occur [21].

The application of our system to the HOG and the p53 system also provides evidence that nested autoinhibitory feedbacks increase the robustness of the steady state with respect to parameter perturbations. For the ERK pathway, it has been observed that a fast post-translational feedback mechanism confers robustness to steady-state phosphorylation of ERK [47], which supports our analysis.

Our results may have implications to understand the complex dynamics of a range of signalling pathways. Not only has the p53 system been shown to exhibit different dynamics depending on the stimulus. The ERK pathway can show both oscillatory and adaptive dynamics, which are likely due to different feedback mechanisms that act on different timescales and that are activated depending on the stimulus [47–49]. The NF-κB system can show damped oscillations, which are likely due to different feedback mechanisms acting on different timescales [27]. It seems that the coupling of fast post-translational and delayed transcriptional feedbacks is a general feature of signalling pathways that allows fine-tuning of dynamics and steady-state features. The role of fast post-translational negative feedbacks in this respect is apparently either to suppress oscillatory behaviour or stabilize steady-state protein levels or both.

The presented theoretical results on suppressing oscillatory behaviour induced by Hopf bifurcations may be useful in designing synthetic systems in which oscillations can be tuned by synthetic autoinhibitory feedbacks. This may be useful for studying cell fate decisions, as, for example, in the p53 or the ERK system. For the HOG system, the parametrized models show that even without autoinhibitory feedback osmo-adaptation is extremely stable. For this system, it seems unlikely that oscillations can be induced artificially by weakening the reported autoinhibitory feedbacks.

4. Material and methods

4.1. Data

We made extensive use of published data to parametrize dynamic models of the HOG pathway and the p53 pathway. The dataset used for model parametrization and discrimination of the HOG model was taken from [17]. This dataset consists of time series of phosphorylated Hog1 under several hyper-osmotic shock conditions, for wild-type and different mutants yeast, for up to 2 h after hyper-osmotic shock (figure 5*a*,*b*). Additionally, we used a time series of glycerol published in [22] (figure 5*c*). These datasets, although coming from different sources, are comparable because they were produced using the same genetic background and under the same culture conditions. The dataset used for model parametrization and discrimination of the p53 model was digitized from the electronic supplementary material, figure S6 of the supplementary material of [25]. These data are meant to resemble an idealized undamped oscillation with peak characteristic that correspond to the average peak characteristic of oscillating cells. For the ranking procedure, we considered only 91 data

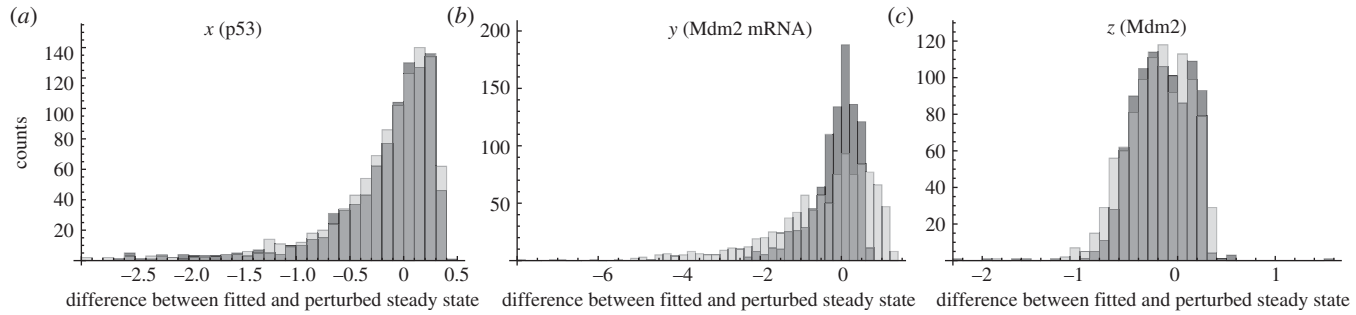

Figure 10. Monte Carlo analysis of the best approximating model with and without autoinhibitory feedback of the p53 system. (*a–c*) Shows the distributions of the difference between the original and the perturbed calculated steady states of the model with autoinhibitory feedback no. 15 (dark grey) and the model without autoinhibitory feedback no. 11 (light grey), respectively, for one of the three model components as indicated in the respective panel title. The dark grey regions indicate overlapping distributions. The free parameters (see electronic supplementary material, table S3) were perturbed by sampling 1000 times from a uniform distribution ranging from half to double of their original values and calculating the according steady states.

points, because the last three periods in figure 8 are repetitions of the former oscillations.

4.2. Model fitting, ranking and selecting

The models were implemented and fitted with the free software COPASI (v. 4.7, build 34) [50]. We used the evolutionary programming algorithm to fit the models, where the population size was set to 10 times the number of parameters and the number of generations was limited to 10 times the number of parameters. When estimated parameters hit parameter boundaries, the boundaries were relaxed and the model refitted until the fit converged within defined parameter boundaries. Model ranking was performed using modelMaGe [51,52]. For model ranking, we calculated the Akaike information criterion corrected (AICc) for small sample sizes [53] for each candidate model:

$$\mathrm{AIC}c = 2k + n\left(\ln\left(\frac{2\pi \mathrm{SSR}}{n}\right) + 1\right) + \frac{2k(k+1)}{n-k-1},$$

where SSR is the sum of squared residuals of the fit, k is the number of parameters and n is the number of data points. The AICc is an information-theory-based measure of parsimonious data representation that incorporates the goodness of the fit (SSR) as well as the complexity of the model (k), thereby giving an objective measure for model selection and discrimination.

In order to select and compare the best approximating model(s), we calculated the Akaike weights (AICw) [53]

$$\mathrm{AIC}w_i = \frac{\mathrm{e}^{-1/2\Delta_i}}{\sum_{r=1}^{R} \mathrm{e}^{-1/2\Delta_r}},$$

where $\Delta_i = \mathrm{AIC}_i - \mathrm{AIC}_{\min}$, with AIC_i being the AICc for model i, $i = 1,\ldots, R$ according to ranking and $\mathrm{AIC}_{\min}$ the minimal AICc. The AICws can be considered as the weight of evidence in favour of a model given as a number between 0 and 1, i.e. the higher the weight, the closer the model is to the hypothetical true model [53]. We considered those models as best approximating that had an AIC$w > 0.125$.

Funding statement. This study was supported by the German Ministry of Science and Education (BMBF project no. 0135779 and 0316188E to J.S.) and the International Max Planck Research School Magdeburg for Advanced Methods in Process and Systems Engineering. The authors declare no conflicting interests.

References

1. Alon U. 2007 Network motifs: theory and experimental approaches. *Nat. Rev. Genet.* **8**, 450–461. (doi:10.1038/nrg2102)
2. Legewie S, Herzel H, Westerhoff HV, Bluthgen N. 2008 Recurrent design patterns in the feedback regulation of the mammalian signalling network. *Mol. Syst. Biol.* **4**, 190. (doi:10.1038/msb.2008.29)
3. Kholodenko BN. 2000 Negative feedback and ultrasensitivity can bring about oscillations in the mitogen-activated protein kinase cascades. *Eur. J. Biochem.* **267**, 1583–1588. (doi:10.1046/j.1432-1327.2000.01197.x)
4. Tyson JJ, Chen KC, Novak B. 2003 Sniffers, buzzers, toggles and blinkers: dynamics of regulatory and signaling pathways in the cell. *Curr. Opin. Cell Biol.* **15**, 221–231. (doi:10.1016/S0955-0674(03)00017-6)
5. Tsai TY, Choi YS, Ma W, Pomerening JR, Tang C, Ferrell Jr JE. 2008 Robust, tunable biological oscillations from interlinked positive and negative feedback loops. *Science* **321**, 126–129. (doi:10.1126/science.1156951)
6. Kholodenko BN, Hancock JF, Kolch W. 2010 Signalling ballet in space and time. *Nat. Rev. Mol. Cell Biol.* **11**, 414–426. (doi:10.1038/nrm2901)
7. Ma W, Trusina A, El-Samad H, Lim WA, Tang C. 2009 Defining network topologies that can achieve biochemical adaptation. *Cell* **138**, 760–773. (doi:10.1016/j.cell.2009.06.013)
8. Yi TM, Huang Y, Simon MI, Doyle J. 2000 Robust perfect adaptation in bacterial chemotaxis through integral feedback control. *Proc. Natl Acad. Sci. USA* **97**, 4649–4653. (doi:10.1073/pnas.97.9.4649)
9. Ni XY, Drengstig T, Ruoff P. 2009 The control of the controller: molecular mechanisms for robust perfect adaptation and temperature compensation. *Biophys. J.* **97**, 1244–1253. (doi:10.1016/j.bpj.2009.06.030)
10. Drengstig T, Jolma IW, Ni XY, Thorsen K, Xu XM, Ruoff P. 2012 A basic set of homeostatic controller motifs. *Biophys. J.* **103**, 2000–2010. (doi:10.1016/j.bpj.2012.09.033)
11. Alon U. 2007 *An introduction to systems biology*. Boca Raton, FL: Chapman and Hall/CRC.
12. Sturm OE *et al*. 2010 The mammalian MAPK/ERK pathway exhibits properties of a negative feedback amplifier. *Sci. Signal.* **3**, ra90. (doi:10.1126/scisignal.2001212)
13. Novak B, Vinod PK, Freire P, Kapuy O. 2010 Systems-level feedback in cell-cycle control. *Biochem. Soc. Trans.* **38**, 1242–1246. (doi:10.1042/BST0381242)
14. Elowitz MB, Leibler S. 2000 A synthetic oscillatory network of transcriptional regulators. *Nature* **403**, 335–338. (doi:10.1038/35002125)
15. Goodwin BC. 1965 Oscillatory behavior in enzymatic control processes. *Adv. Enzyme Regul.* **3**, 425–438. (doi:10.1016/0065-2571(65)90067-1)
16. Griffith JS. 1968 Mathematics of cellular control processes. I. Negative feedback to one gene. *J. Theor. Biol.* **20**, 202–208. (doi:10.1016/0022-5193(68)90189-6)
17. Macia J, Regot S, Peeters T, Conde N, Sole R, Posas F. 2009 Dynamic signaling in the Hog1 MAPK pathway relies on high basal signal

transduction. *Sci. Signal.* **2**, ra13. (doi:10.1126/scisignal.2000056)

18. Ferrell Jr JE, Tsai TY, Yang Q. 2011 Modeling the cell cycle: why do certain circuits oscillate? *Cell* **144**, 874–885. (doi:10.1016/j.cell.2011.03.006)
19. Kollmann M, Lovdok L, Bartholome K, Timmer J, Sourjik V. 2005 Design principles of a bacterial signalling network. *Nature* **438**, 504–507. (doi:10.1038/nature04228)
20. Bluthgen N. 2010 Transcriptional feedbacks in mammalian signal transduction pathways facilitate rapid and reliable protein induction. *Mol. Biosyst.* **6**, 1277–1284. (doi:10.1039/c002598d)
21. Schaber J, Baltanas R, Bush A, Klipp E, Colman-Lerner A. 2012 Modelling reveals novel roles of two parallel signalling pathways and homeostatic feedbacks in yeast. *Mol. Syst. Biol.* **8**, 622. (doi:10.1038/msb.2012.53)
22. Klipp E, Nordlander B, Kruger R, Gennemark P, Hohmann S. 2005 Integrative model of the response of yeast to osmotic shock. *Nat. Biotechnol.* **23**, 975–982. (doi:10.1038/nbt1114)
23. Mahaffy JM, Pao CV. 1984 Models of genetic control by repression with time delays and spatial effects. *J. Math Biol.* **20**, 39–57. (doi:10.1007/BF00275860)
24. Lahav G, Rosenfeld N, Sigal A, Geva-Zatorsky N, Levine AJ, Elowitz MB, Alon U. 2004 Dynamics of the p53-Mdm2 feedback loop in individual cells. *Nat. Genet.* **36**, 147–150. (doi:10.1038/ng1293)
25. Geva-Zatorsky N *et al*. 2006 Oscillations and variability in the p53 system. *Mol. Syst. Biol.* **2**, 20060033. (doi:10.1038/msb4100068)
26. Purvis JE, Karhohs KW, Mock C, Batchelor E, Loewer A, Lahav G. 2012 p53 dynamics control cell fate. *Science* **336**, 1440–1444. (doi:10.1126/science.1218351)
27. Hoffmann A, Levchenko A, Scott ML, Baltimore D. 2002 The IκB-NF-κB signaling module: temporal control and selective gene activation. *Science* **298**, 1241–1245. (doi:10.1126/science.1071914)
28. Nelson DE *et al*. 2004 Oscillations in NF-κB signaling control the dynamics of gene expression. *Science* **306**, 704–708. (doi:10.1126/science.1099962)
29. Ashall L *et al*. 2009 Pulsatile stimulation determines timing and specificity of NF-κB-dependent transcription. *Science* **324**, 242–246. (doi:10.1126/science.1164860)
30. Holling CS. 1973 Resilience and stability of ecological systems. *Annu. Rev. Ecol. Syst.* **4**, 1–23. (doi:10.1146/annurev.es.04.110173.000245)
31. Harrison GW. 1979 Stability under environmental stress: resistance, resilience, persistence, and variability. *Am. Nat.* **113**, 659–669. (doi:10.1086/283424)
32. Nguyen LK. 2012 Regulation of oscillation dynamics in biochemical systems with dual negative feedback loops. *J. R. Soc. Interface* **9**, 1998–2010. (doi:10.1098/rsif.2012.0028)
33. Hohmann S. 2002 Osmotic stress signaling and osmoadaptation in yeasts. *Microbiol. Mol. Biol. Rev.* **66**, 300–372. (doi:10.1128/MMBR.66.2.300-372.2002)
34. Zi Z, Liebermeister W, Klipp E. 2010 A quantitative study of the Hog1 MAPK response to fluctuating osmotic stress in *Saccharomyces cerevisiae*. *PLoS ONE* **5**, e9522. (doi:10.1371/journal.pone.0009522)
35. Gennemark P, Nordlander B, Hohmann S, Wedelin D. 2006 A simple mathematical model of adaptation to high osmolarity in yeast. *In Silico Biol.* **6**, 193–214.
36. Tamas MJ, Rep M, Thevelein JM, Hohmann S. 2000 Stimulation of the yeast high osmolarity glycerol (HOG) pathway: evidence for a signal generated by a change in turgor rather than by water stress. *FEBS Lett.* **472**, 159–165. (doi:10.1016/S0014-5793(00) 01445-9)
37. Schaber J *et al*. 2010 Biophysical properties of *Saccharomyces cerevisiae* and their relationship with HOG pathway activation. *Eur. Biophys. J.* **39**, 1547–1556. (doi:10.1007/s00249-010-0612-0)
38. Schaber J, Klipp E. 2008 Short-term volume and turgor regulation in yeast. *Essays Biochem.* **45**, 147–159. (doi:10.1042/BSE0450147)
39. Hucka M *et al*. 2003 The systems biology markup language (SBML): a medium for representation and exchange of biochemical network models. *Bioinformatics* **19**, 524–531.
40. Horn HF, Vousden KH. 2007 Coping with stress: multiple ways to activate p53. *Oncogene* **26**, 1306–1316. (doi:10.1038/sj.onc.1210263)
41. Batchelor E, Loewer A, Lahav G. 2009 The ups and downs of p53: understanding protein dynamics in single cells. *Nat. Rev. Cancer* **9**, 371–377. (doi:10.1038/nrc2604)
42. Batchelor E, Loewer A, Mock C, Lahav G. 2011 Stimulus-dependent dynamics of p53 in single cells. *Mol. Syst. Biol.* **7**, 488. (doi:10.1038/msb.2011.20)
43. Batchelor E, Mock CS, Bhan I, Loewer A, Lahav G. 2008 Recurrent initiation: a mechanism for triggering p53 pulses in response to DNA damage. *Mol. Cell* **30**, 277–289. (doi:10.1016/j.molcel.2008.03.016)
44. Santos SD, Verveer PJ, Bastiaens PI. 2007 Growth factor-induced MAPK network topology shapes Erk response determining PC-12 cell fate. *Nat. Cell Biol.* **9**, 324–330. (doi:10.1038/ncb1543)
45. Cai L, Dalal CK, Elowitz MB. 2008 Frequency-modulated nuclear localization bursts coordinate gene regulation. *Nature* **455**, 485–490. (doi:10.1038/nature07292)
46. Bliss RD, Painter PR, Marr AG. 1982 Role of feedback inhibition in stabilizing the classical operon. *J. Theor. Biol.* **97**, 177–193. (doi:10.1016/0022-5193(82)90098-4)
47. Fritsche-Guenther R, Witzel F, Sieber A, Herr R, Schmidt N, Braun S, Brummer T, Sers C, Bluthgen N. 2011 Strong negative feedback from Erk to Raf confers robustness to MAPK signalling. *Mol. Syst. Biol.* **7**, 489. (doi:10.1038/msb.2011.27)
48. Cirit M, Wang CC, Haugh JM. 2010 Systematic quantification of negative feedback mechanisms in the extracellular signal-regulated kinase (ERK) signaling network. *J. Biol. Chem.* **285**, 36 736–36 744. (doi:10.1074/jbc.M110.148759)
49. Shankaran H, Ippolito DL, Chrisler WB, Resat H, Bollinger N, Opresko LK, Wiley HS. 2009 Rapid and sustained nuclear-cytoplasmic ERK oscillations induced by epidermal growth factor. *Mol. Syst. Biol.* **5**, 332. (doi:10.1038/msb.2009.90)
50. Hoops S *et al*. 2006 COPASI: a complex pathway simulator. *Bioinformatics* **22**, 3067–3074. (doi:10.1093/bioinformatics/btl485)
51. Schaber J, Flottmann M, Li J, Tiger CF, Hohmann S, Klipp E. 2011 Automated ensemble modeling with modelMaGe: analyzing feedback mechanisms in the Sho1 branch of the HOG pathway. *PLoS ONE* **6**, e14791. (doi:10.1371/journal.pone.0014791)
52. Flottmann M, Schaber J, Hoops S, Klipp E, Mendes P. 2008 ModelMage: a tool for automatic model generation, selection and management. *Genome Inform.* **20**, 52–63. (doi:10.1142/9781848163003_0005)
53. Burnham KP, Anderson DR. 2002 *Model selection and multi-model inference: a practical information-theoretic approach*. New York, NY: Springer.

Nested auto-inhibitory feedbacks alter the resistance of homeostatic adaptive biochemical networks

Jörg Schaber[1,*], Anastasiya Lapytsko[1], Dietrich Flockerzi[2]

1 Institute for Experimental Internal Medicine, Otto-von-Guericke University, Magdeburg, Germany
2 Max Planck Institute for the Dynamics of Complex Technical Systems, Magdeburg, Germany
∗ **E-mail: schaber@med.ovgu.de**

1 Hopf bifurcation

1.1 The model

With positive parameters k_0, k_1, k_2, k_3, k_4, k_5, and k_6 we consider a class of smooth 3D-systems of the form

$$\begin{aligned}\frac{dx}{dt} &= k_0\, q(z) - \Big(k_1\, f_0(x) + k_2\, F(x,z)\Big)\,,\\ \frac{dy}{dt} &= k_3\, f_2(x)\, G(y) - k_4\, g_1(y)\,,\\ \frac{dz}{dt} &= k_5\, g_2(y)\, H(z) - k_6\, h(z)\,.\end{aligned} \tag{1.1}$$

for non-negative initial values $x(0), y(0)$ and $z(0)$. We assume f_0, f_2, g_1, g_2 and h to be strictly increasing functions on $\mathbb{R}_{\geq 0}$ vanishing at 0. The smooth function $F(x,z)$ is to be non-negative on $\mathbb{R}^2_{\geq 0}$ and to vanish on the boundary of $\mathbb{R}^2_{\geq 0}$. Moreover, the partial derivatives F_x and F_z are assumed to be non-negative on $\mathbb{R}^2_{\geq 0}$. The function $q(z)$ is a smooth, positive and strictly decreasing function with $q(0) = 1$, the function $H(z)$ is alike. Finally, the function $G(y)$ is

$$G(y) = (y_T - y)\, g(y) \quad \text{or} \tag{1.2a}$$

$$G(y) = g(y) \tag{1.2b}$$

with $g(y)$ being either identically 1 or a smooth, positive and strictly decreasing function with $g(0) = 1$, and, in case of (1.2a), for a positive parameter y_T. Note that the non-negative orthant $\mathbb{R}^3_{\geq 0}$ and, more specifically, $Q = \{0 \leq x \leq k_0/k_1, 0 \leq y, 0 \leq z\}$ is positive invariant.

The model (1.1) with $G(y)$ of the form (1.2a) represents a model with an a-priori bound $y \leq y_T$ for the second solution component in case its initial value $y(0)$ is in $[0, y_T]$. This represents a reduced 4-dimensional $(x, y, \widetilde{y}, z)$-system with $y_T = y + \widetilde{y}$, mimicking post-translational modifications of a protein y without affecting the total protein abundance y_T. We will refer to a model with $G(y)$ of the form (1.2a) to a model with signalling component. Note that

$$Q_T = \{0 \leq x \leq k_0/k_1, 0 \leq y \leq y_T, 0 \leq z\}$$

is positive invariant in this case. All general results hold for both types of $G(y)$, however, we will mainly consider models where $G(y)$ is of the form (1.2a).

The functions $g(y)$, and $H(z)$ represent auto-inhibitory feedbacks, whereas the functions $q(z)$ and $F(x,z)$ represent delayed negative feedbacks. The feedback $q(z)$ is inhibiting the inflow reaction, as in

the classical model of Goodwin [1, 2], whereas the feedback $F(x, z)$ is activating the outflow reaction for the species x. In the special cases considered in 2.1 and 2.2, both for the auto-inhibitory as well as for the delayed negative feedbacks, only one of these feedbacks is considered to be active at a time.

1.2 The steady state

Any steady state $\hat{E} = (\hat{x}, \hat{y}, \hat{z})^T$ of (1.1) in $\mathbb{R}^3_{\geq 0}$ is given by

$$\hat{y} = Y(\hat{z}) := g_2^{-1}\Big(\frac{k_6\, h(\hat{z})}{k_5\, H(\hat{z})}\Big)\,, \quad \hat{x} = X(\hat{z}) := f_2^{-1}\Big(\frac{k_4\, g_1(Y(\hat{z}))}{k_3\, G(Y(\hat{z}))}\Big) \tag{1.3}$$

for the parameter value

$$\hat{k}_0 = P(\hat{z}, k_1) := \frac{1}{q(\hat{z})}\,\Big(k_1\, f_0(X(\hat{z})) + k_2\, F(X(\hat{z}), \hat{z})\Big)\,. \tag{1.4}$$

provided the inverses g_2^{-1} and f_2^{-1} exist (including the condition $G(Y(\hat{z})) > 0$), i.e., provided $\dfrac{k_6\, h(\hat{z})}{k_5\, H(\hat{z})}$ is in the range of g_2 and $\dfrac{k_4\, g_1(Y(\hat{z}))}{k_3\, G(Y(\hat{z}))}$ is in the range of f_2. Note that X and Y in (1.3) are strictly increasing functions of $\hat{z}$. Hence P is strictly increasing in $\hat{z}$ as well as in k_1. Thus, there is a 1-1 correspondence between the parameter $\hat{k}_0$ and the third component of the equilibrium $\hat{E}$. For models with $G(y)$ being of the form (1.2a) and steady states in Q_T, the $\hat{z}$ is to be in $(0, q_T]$ with $Y(q_T) = y_T$. Consequently, $\hat{k}_0$ ranges in $(0, P(q_T, k_1)]$ and the steady state $\hat{E}$ is unique in Q_T.

The Jacobian at equilibrium $\hat{E} = (\hat{x}, \hat{y}, \hat{z})^T$ is of the form

$$\begin{aligned} J(\hat{z}, k_1) &= \begin{bmatrix} -A & 0 & -B \\ C & -D & 0 \\ 0 & E & -F \end{bmatrix} \\ &:= \begin{bmatrix} -\Big[k_1 f_0'(\hat{x}) + k_2\, F_x(\hat{x}, \hat{z})\Big] & 0 & -\Big[\hat{k}_0 |q'(\hat{z})| + k_2\, F_z(\hat{x}, \hat{z})\Big] \\ k_3\, f_2'(\hat{x}) G(\hat{y}) & -\Big[k_3\, f_2(\hat{x})\, |G'(\hat{y})| + k_4 g_1'(\hat{y})\Big] & 0 \\ 0 & k_5 g_2'(\hat{y})\, H(\hat{z}) & -\Big[k_5\, g_2(\hat{y})\, |H'(\hat{z})| + k_6\, h'(\hat{z})\Big] \end{bmatrix}. \end{aligned} \tag{1.5}$$

Thus, at a positive fixed point $\hat{E}$, one has the characteristic polynomial

$$det(\lambda\, I - J(\hat{z}, k_1)) = \lambda^3 + \Delta_2 \lambda^2 + \Delta_1 \lambda + \Delta_0$$

with positive

$$\Delta_2 = A + D + F, \quad \Delta_1 = AD + AF + DF, \quad \Delta_0 = ADF + BCE\ .$$

So, any real eigenvalue of $J(\hat{z}, k_1)$ is negative. The necessary and sufficient condition for a single pair $\pm i\omega = \pm i\sqrt{\Delta_1}$ of pure imaginary eigenvalues ($\omega > 0$) is $\Delta_0 = \Delta_1 \Delta_2$, i.e.,

$$BCE = (D + F)\big(A^2 + A(D + F) + DF\big) \tag{1.6}$$

evaluated at $\hat{E}$. With

$$\begin{aligned} A =& k_1\, A_1 + A_0, \quad A_1 := f_0'(X(\hat{z}))\,,\ A_0 := k_2 F_x(X(\hat{z}), \hat{z})\,, \quad \text{and} \\ B =& k_1\, B_1 + B_0, \quad B_1 := f_0(X(\hat{z}))\frac{|q'(\hat{z})|}{q(\hat{z})}\,,\ B_0 := k_2\, F(X(\hat{z}), \hat{z})\frac{|q'(\hat{z})|}{q(\hat{z})} + k_2 F_z(X(\hat{z}), \hat{z})\,, \end{aligned}$$

we consider (1.6) as an equation of the parameters k_1 and $\hat{z}$ that is to be solved in the form $k_1 = K_1(\hat{z})$. The curve $K_1(\hat{z})$, given by the unique positive solution $k_1 = K_1(\hat{z})$ of the quadratic equation – derived from (1.6) –

$$\begin{aligned} &k_1^2 A_1^2 + k_1\, R_1(\hat{z}) - R_0(\hat{z}) = \\ &k_1^2 A_1^2 + k_1 \Big(2\, A_0 A_1 + A_1(D+F) - \frac{B_1 CE}{D+F}\Big) + \big(A_0 + D\big)\big(A_0 + F\big) - \frac{B_0 CE}{D+F} = 0 \end{aligned} \tag{1.7}$$

evaluated at $\hat{E}$, indicates possible Hopf bifurcation points in the $\hat{z}$-k_1-plane. The necessary and sufficient condition of the existence for a positive solution k_1 of (1.7) is $R_0(\hat{z}) \overset{!}{>} 0$, i.e.,

$$B_0 CE \overset{!}{>} (D+F)(A_0+D)(A_0+F)\,. \tag{1.8}$$

Taken together, having chosen the equilibrium component $\hat{z}$, we define $\hat{x}$, $\hat{y}$ according to (1.3) and solve (1.7) for $k_1 = K_1(\hat{z}) > 0$, provided (1.8) is satisfied, and set $\hat{k}_0 = P(\hat{z}, k_1)$ according to (1.4). Then, the possible Hopf-point is given by $\hat{E} = (\hat{x}, \hat{y}, \hat{z})^T$ for the critical parameters $k_1^{crit} = K_1(\hat{z})$ and $\hat{k}_0^{crit} = P(\hat{z}, k_1^{crit})$.

1.3 Hopf Transversality Condition

It rests to show that the above defined candidate bifurcation point $\hat{E} = (X(\hat{z}), Y(\hat{z}), \hat{z})^T$ satisfies the transversality condition of the critical eigenvalues $\lambda_{1,2}(k_1) = \mu(k_1) \pm i\omega(k_1)$ of (1.5), i.e.,

$$\mu'(k_1^{crit}) = \left.\frac{\partial \mu(k_1)}{\partial k_1}\right|_{k_1 = k_1^{crit}} \neq 0\,, \quad {}' = \frac{\partial}{\partial k_1}\,,$$

with $\mu(k_1^{crit}) = 0$ and $\omega(k_1^{crit}) > 0$ suppressing the $\hat{z}$-dependence for the moment.
With

$$\omega = \pm\sqrt{A\,D + D\,F + A\,F}$$

and (1.6) the vectors

$$v = (-BE, (A+i\omega)(F+i\omega), E(A+i\omega))^T, \quad w^* = (C(F+i\omega), (A+i\omega)(F+i\omega), -BC)\,,$$

are right and left eigenvectors of $J(k_1^{crit})$, respectively.
With $J(k_1^{crit})v = (\mu(k_1^{crit}) + i\omega(k_1^{crit}))\, v$ we compute an expression for $\mu'(k_1^{crit})$ as follows:

$$J'(k_1^{crit})\, v + J(k_1^{crit})\, v' = (\mu'(k_1^{crit}) + i\omega'(k_1^{crit}))\, v + (\mu(k_1^{crit}) + i\omega(k_1^{crit}))\, v'\,.$$

Left-multiplication with w^* and inserting $\mu(k_1^{crit}) = 0$ lead to

$$w^*\, J'(k_1^{crit})\, v - i\,\omega(k_1^{crit})\, w^*\, v' = (\mu'(\,k_1^{crit}) + i\omega'(k_1^{crit}))\, w^*\, v + (\mu(k_1^{crit}) + i\omega(k_1^{crit}))\, w^*\, v'\,. \tag{1.9}$$

Apparently one has $J'(k_1^{crit}) = -f_0'(\hat{x}) e_1 e_1^T - f_0(\hat{x}) \dfrac{|q'(\hat{z})|}{q(\hat{z})} e_1 e_3^T$. Thus, taking the real part of (1.9) one obtains

$$\begin{aligned} \mu' =& Re\Big(\frac{w^*\, J'\, v}{w^*\, v}\Big) \;=\; Re\Big(\frac{(D+i\omega)(F+i\omega)\,(-Bq(\hat{z})f_0'(\hat{x}) + (A+i\omega)f_0(\hat{x})\,|q'(\hat{z})|)}{Bq(\hat{z})\,(2i\omega(A+D+F) + AD + AF + DF - 3\omega^2)}\Big) \\ =& \frac{(D+F)(A(D+F)+DF)\,((A+D)(A+F)\,|q'(\hat{z})|\,f_0(\hat{x}) - Bq(\hat{z})(2A+D+F)f_0'(\hat{x}))}{2Bq(\hat{z})\,(\omega^2(A+D+F)^2 + (A(D+F)+DF)^2)} \\ =& \frac{(D+F)\Delta_1\,((A+D)(A+F)\,|q'(\hat{z})|\,f_0(\hat{x}) - Bq(\hat{z})(2A+D+F)f_0'(\hat{x}))}{2B\,(\Delta_1^2 + \Delta_2^2\Delta_1)\,q(\hat{z})} \\ =& f_0(\hat{x})\frac{|q'(\hat{z})|}{q(\hat{z})}\frac{CE}{2\,(\Delta_2^2 + \Delta_1)} - f_0'(\hat{x})\frac{(A+\Delta_2)\,(D+F)}{2\,(\Delta_2^2+\Delta_1)} \neq 0 \quad \text{at} \;\; (\hat{z}, K_1(\hat{z}))\,. \end{aligned}$$

Thus the transversality condition $\mu' \neq 0$ for a Hopf bifurcation is generically fulfilled. Whether a supercritical or subcritical Hopf bifurcation occurs can be calculated with the Lyapunov coefficient, but should only be evaluated for concrete cases. In the cases considered below, the system (1.1) exhibits subcritical Hopf bifurcations [3].

2 The role of auto-inhibitory feedback functions g and H

In the present section, we consider systems in which

$$f_0(x) = f_2(x) = x \quad \text{and} \quad g_1(y) = g_2(y) = y \tag{2.1}$$

and the auto-inhibitory feedback functions g and H have the form

$$g(y, \kappa_y) = \frac{1}{1 + \kappa_y\, y^m} \quad \text{and} \tag{2.2a}$$

$$H(z, \kappa_z) = \frac{1}{1 + \kappa_z\, z^n}\ , \tag{2.2b}$$

respectively. Here, one has

$$\begin{aligned} H'(z, \kappa_z) :=& \frac{\partial}{\partial z}\Big(\frac{1}{1 + \kappa_z\, z^n}\Big) = -n\, \kappa_z\, z^{n-1} H^2(z, \kappa_z) \text{ and} \\ & \frac{\partial}{\partial \kappa_z} H(z, \kappa_z) = -z^n H^2(z, \kappa_z)\ . \end{aligned} \tag{2.3}$$

and for $G(y, \kappa_y) = (y_T - y) g(y, \kappa_y)$ from (1.2),

$$\begin{aligned} G'(y, \kappa_y) :=& \frac{\partial G}{\partial y}(y, \kappa_y) = -\Big[\kappa_y\, m\, y^{m-1}\, g^2(y, \kappa_y)(y_T - y) + g(y, \kappa_y)\Big] \\ \text{and} \quad & |G'(y, \kappa_y)| = \kappa_y\, m\, y^{m-1}\, g^2(y, \kappa_y)(y_T - y) + g(y, \kappa_y)\ >\ 0\,, \\ & \frac{\partial}{\partial \kappa_y} G(y, \kappa_y) = -(y_T - y) y^m g^2(z, \kappa_y)\ . \end{aligned} \tag{2.4}$$

We are interested in the κ_y- and κ_z-dependence of the stability of the steady state of the system (1.1), respectively. Thus, in the following, we list κ_y and κ_z as additional parameters in the relevant expressions. Note that in the two considered cases below we analyse only one of the functions $g(y, \kappa_y)$ and $H(z, \kappa_z)$ at a time, whereas the remaining function is considered to be identically 1.

As above, we assume $G(y, \kappa_y) = (y_T - y)\, g(y, \kappa_y)$ and $0 \le y \le y_T$, but all general results can also be derived for the case $G(y, \kappa_y) = g(y, \kappa_y)$. In addition, we assume the function $F(x, z)$ to be of the form

$$F(x, z) = f_1(x)\, f_3(z) = \frac{x}{K_x + x} f_3(z)\ , \tag{2.5}$$

with strictly increasing f_3 on $\mathbb{R}_{\ge 0}$ vanishing at 0.

Apparently, we can always decrease K_x such that one has $f_1(\hat{x}) \approx 1$ at the equilibrium $\hat{E} = (\hat{x}, \hat{y}, \hat{z})^T = (X(\hat{z}), Y(\hat{z}), \hat{z})^T$ (cf. (1.3)). Thus, we further approximate f_1 by a smooth $f_1 : [0, \infty) \to [0, 1]$ with

$$f_1(0) = 0\,, \quad f_1(x) = 1 \ \text{ for } x \ge a > 0 \ \text{ strictly increasing on } (0, a)$$

and require that the x-component of the equilibrium $\hat{E}$ fulfills

$$\hat{x} = X(\hat{z}, \kappa) > a \text{ and thus } f_1(X(\hat{z}, \kappa)) = 1\ , f_1'(X(\hat{z}, \kappa)) = \frac{\partial f_1}{\partial x}(X(\hat{z}, \kappa)) = 0\,. \tag{2.6}$$

Hence, in this case is $F_x(x, z) = 0$ and $F(\hat{x}, \hat{z}) = f_3(\hat{z})$.

2.1 The κ_y-dependence of the bifurcation curve $K_1(\hat{z})$

We consider (1.1) with (2.1), where $g(y,\kappa_y)$ is of the form (2.2a), $H \equiv 1$, and $F(x,z) = f_1(x)\, f_3(z)$ with f_1 satisfying (2.6). Thus system 1.1 becomes

$$\begin{aligned} \frac{dx}{dt} &= k_0\, q(z) - \Big(k_1\, x + k_2\, f_1(x)\, f_3(z)\Big)\,, \\ \frac{dy}{dt} &= k_3\, x\, G(y,\kappa_y) - k_4\, y\,, \\ \frac{dz}{dt} &= k_5\, y - k_6\, h(z)\,. \end{aligned} \tag{2.7}$$

In this case, the equilibrium functions (1.3) read

$$\hat{y} = Y(\hat{z}) := \frac{k_6\, h(\hat{z})}{k_5} \le y_T\,, \quad \hat{x} = X(\hat{z},\kappa_y) := \frac{k_4\, Y(\hat{z})}{k_3\, G(Y(\hat{z}),\kappa_y)} \tag{2.8}$$

for the parameter value

$$\hat{k}_0 = P(\hat{z}, k_1, \kappa_y) := \frac{1}{q(\hat{z})}\,\Big(k_1\, X(\hat{z},\kappa_y) + k_2\, f_3(\hat{z})\Big)\,. \tag{2.9}$$

With (2.6) the Jacobian of (2.7) at the steady state $\hat{E}$ is given by

$$\begin{aligned} J(\hat{z},k_1,\kappa_y) &= \begin{bmatrix} -k_1 & 0 & -B(k_1,\hat{z},\kappa_y) \\ C(\hat{z},\kappa_y) & -D(\hat{z},\kappa_y) & 0 \\ 0 & E & -F(\hat{z}) \end{bmatrix} \\ &:= \begin{bmatrix} -k_1 & 0 & -(k_1\, B_1(\hat{z},\kappa_y) + B_0(\hat{z})) \\ k_3\, G(Y(\hat{z}),\kappa_y) & -[k_4 + k_3\, X(\hat{z},\kappa_y)\, |G'(Y(\hat{z}),\kappa_y)|] & 0 \\ 0 & k_5 & -k_6\, h'(\hat{z}) \end{bmatrix} \\ &= \begin{bmatrix} -k_1 & 0 & -(k_1\, B_1(\hat{z},\kappa_y) + B_0(\hat{z})) \\ k_3\, G(Y(\hat{z}),\kappa_y) & -k_4\,[1 + Y(\hat{z})\, \frac{|G'(Y(\hat{z}),\kappa_y)|}{G(Y(\hat{z}),\kappa_y)}] & 0 \\ 0 & k_5 & -k_6\, h'(\hat{z}) \end{bmatrix} \end{aligned} \tag{2.10}$$

where

$$\begin{aligned} B_0(\hat{z}) &= k_2\, f_3(\hat{z}) \frac{|q'(\hat{z})|}{q(\hat{z})} + k_2\, f_3'(\hat{z}) \quad \text{and} \\ B_1(\hat{z},\kappa_y) &= X(\hat{z},\kappa_y) \frac{|q'(\hat{z})|}{q(\hat{z})}\,. \end{aligned} \tag{2.11}$$

Thus, according to (1.7), the critical curve $k_1 = K_1(\hat{z},\kappa_y)$ becomes – for fixed κ_y – the unique positive solution of the quadratic equation

$$0 = k_1^2 + R_1(\hat{z},\kappa_y)\, k_1 - R_0(\hat{z},\kappa_y)\,. \tag{2.12}$$

Note that, with (2.11) and (2.8), $B_1(\hat{z},\kappa_y)\, C(\hat{z},\kappa_y)\, E = k_4\, k_5\, Y(\hat{z}) \frac{|q'(\hat{z})|}{q(\hat{z})}$, such that the coefficients of (2.12) become

$$\begin{aligned} R_1(\hat{z},\kappa_y) =& D(\hat{z},\kappa_y) + F(\hat{z}) - \frac{k_4\, k_5\, Y(\hat{z})}{D(\hat{z},\kappa_y) + F(\hat{z})}\, \frac{|q'(\hat{z})|}{q(\hat{z})} \quad \text{and} \\ R_0(\hat{z},\kappa_z) =& \frac{B_0(\hat{z})\, C(\hat{z},\kappa_y)\, E}{D(\hat{z},\kappa_y) + F(\hat{z})} - D(\hat{z},\kappa_y)\, F(\hat{z})\,, \end{aligned}$$

We are interested in the κ_y-dependence of the positive solutions $k_1 = K_1(\hat{z}, \kappa_y)$ of (2.12). Therefore, in the following, we will omit the $\hat{z}$-dependence in some instances for simplicity. With (2.4) and (2.8) one has

$$\begin{aligned} C(\kappa_y) =& k_3\, G(\hat{y}, \kappa_y)\,, \\ D(\kappa_y) =& k_4 \Big[1 + \frac{\hat{y}\,|G'(\hat{y}, \kappa_y)|}{G(\hat{y}, \kappa_y)}\Big] = k_4 \Big[1 + \Big(\frac{\hat{y}}{y_T - \hat{y}} + m\,\kappa_y\,\hat{y}^m\, g(\hat{y}, \kappa_y)\Big)\Big]\,. \end{aligned}$$

Thus, the κ_y-derivatives of $C(\kappa_y)$ and $D(\kappa_y)$ are given by

$$\begin{aligned} C'(\kappa_y) &= -k_3\,(y_T - \hat{y})\,\hat{y}^m\, g^2(\hat{y}, \kappa_y) \;<\; 0 \\ D'(\kappa_y) &= k_4\, m\,\hat{y}^m\, g^2(\hat{y}, \kappa_y) \;>\; 0 \end{aligned} \tag{2.13}$$

so that the κ_y-derivatives of $R_1(\kappa_y)$ and $R_0(\kappa_y)$ satisfy

$$\begin{aligned} R_1'(\kappa_y) &= D'(\kappa_y) + \frac{k_4\, k_5\, Y\, D'(\kappa_y)}{\big(D(\kappa_y) + F\big)^2}\,\frac{|q'|}{q} \;>\; 0 \quad \text{and} \\ R_0'(\kappa_y) &= \frac{B_0\, C'(\kappa_y)\, E}{D(\kappa_y) + F} - \frac{B_0\, C(\kappa_y)\, E\, D'(\kappa_y)}{\big(D(\kappa_y) + F\big)^2} - D'(\kappa_y)\, F \;<\; 0\,. \end{aligned} \tag{2.14}$$

Under $R_0(\hat{z}, \kappa_y) > 0$, the positive zero $k_1 = K_1(\hat{z}, \kappa_y)$ of (2.12) satisfies

$$\Big(2K_1(\hat{z}, \kappa_y) + R_1(\hat{z}, \kappa_y)\Big)\,\frac{\partial}{\partial \kappa_y} K_1(\hat{z}, \kappa_y) \;=\; R_0'(\hat{z}, \kappa_y) - K_1(\hat{z}, \kappa_y)\, R_1'(\hat{z}, \kappa_y)$$

together with (2.14) leading to

$$\frac{\partial}{\partial \kappa_y} K_1(\hat{z}, \kappa_y) \;<\; 0$$

and thus to a shrinking oscillation region in the $(\hat{z}, k_1)$-plane for increasing κ_y.

2.1.1 Example 1: Outflow-activation model with auto-inhibition in the y-component

For illustration, we set $f_1(x) = x/(K_x + x)$, $f_3(z) = z$ and $h(z) = z/(K_z + z)$. Together with the above introduced specifications (2.1), $g(y, \kappa_y) = 1/(1 + \kappa_y\, y^m)$, and $H \equiv 1$ our system (1.1) becomes

$$\begin{aligned} \frac{dx}{dt} &= k_0 \;- \Big(k_1\, x + \frac{k_2\, x\, z}{K_x + x}\Big) \\ \frac{dy}{dt} &= \frac{k_3\, x\,(y_T - y)}{1 + \kappa_y\, y^m} - k_4\, y \\ \frac{dz}{dt} &= k_5\, y - \frac{k_6\, z}{K_z + z}\;. \end{aligned} \tag{2.15}$$

The corresponding wiring scheme of the system (2.15) is represented in Figure S1A.

In Figure S2A we display the curve $K_1(\hat{z}, \kappa_y)$ according to (2.12) with (2.8) and (2.9) for $\kappa_y = 0$ and $\kappa_y = 40$, respectively.

The dot in Figure S2A indicates a chosen $\hat{z}$ and k_1, for which the corresponding eigenvalues of (2.10) are displayed in Figure S2B for $\kappa_y = 0$ and $\kappa_y = 40$, respectively. Figures S2C and S2D display simulations of (2.15) for the chosen $\hat{z}$ and k_1 and for $\kappa_y = 0$ and $\kappa_y = 40$, respectively. For the other parameter settings refer to the legend in Figure S2. Note that here $f_1(X(\hat{z}, 0)) \approx f_1(X(\hat{z}, 40)) > 0.99 \approx 1$.

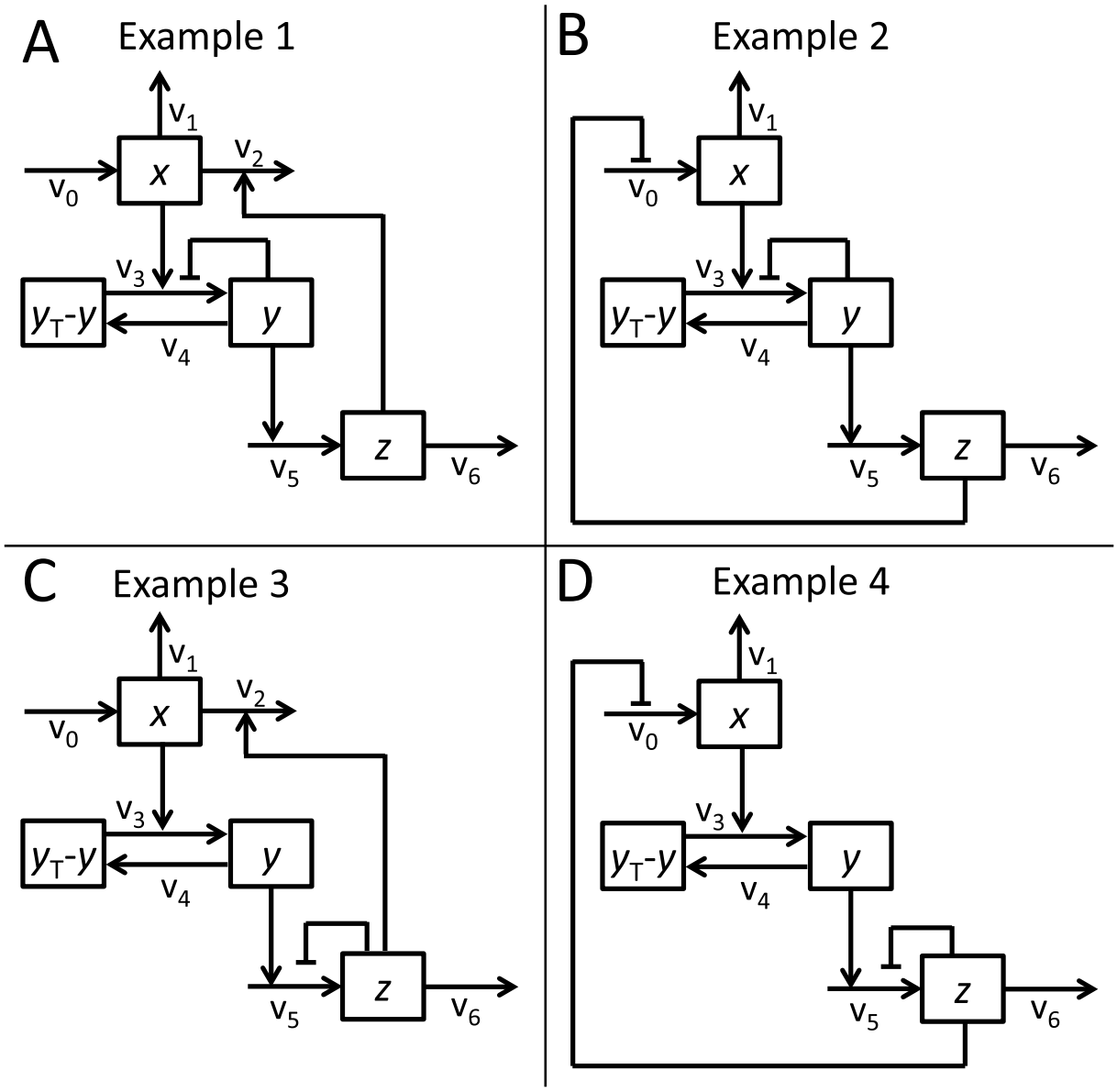

Figure S1 – Wiring schemes of generic integral feedback models. **A**: Outflow-activation model with auto-inhibition in the y-component (Example 1) with equations (2.15), **B**: Inflow-inhibition model with auto-inhibition in the y-component (Example 2) with equations (2.16), **C**: Outflow-activation model with auto-inhibition in the z-component (Example 3) with equations (2.27), **D**: Inflow-inhibition model with auto-inhibition in the z-component (Example 4) with equations (2.28). Reaction numbers correspond to parameter numbers.

Figure S2 shows that, according to the subcritical Hopf bifurcation, the area below the curve $K_1(\hat{z}, \kappa_y)$ is the region, where the system oscillates. Figure S2A also clearly demonstrates that increasing κ_y decreases this region. Thus, for given values of $\hat{z}$ and k_1, we can increase κ_y such that the initially oscillating system (Figure S2C) is stabilized (Figure S2D), corresponding to a shift of the single pair of pure imagi-

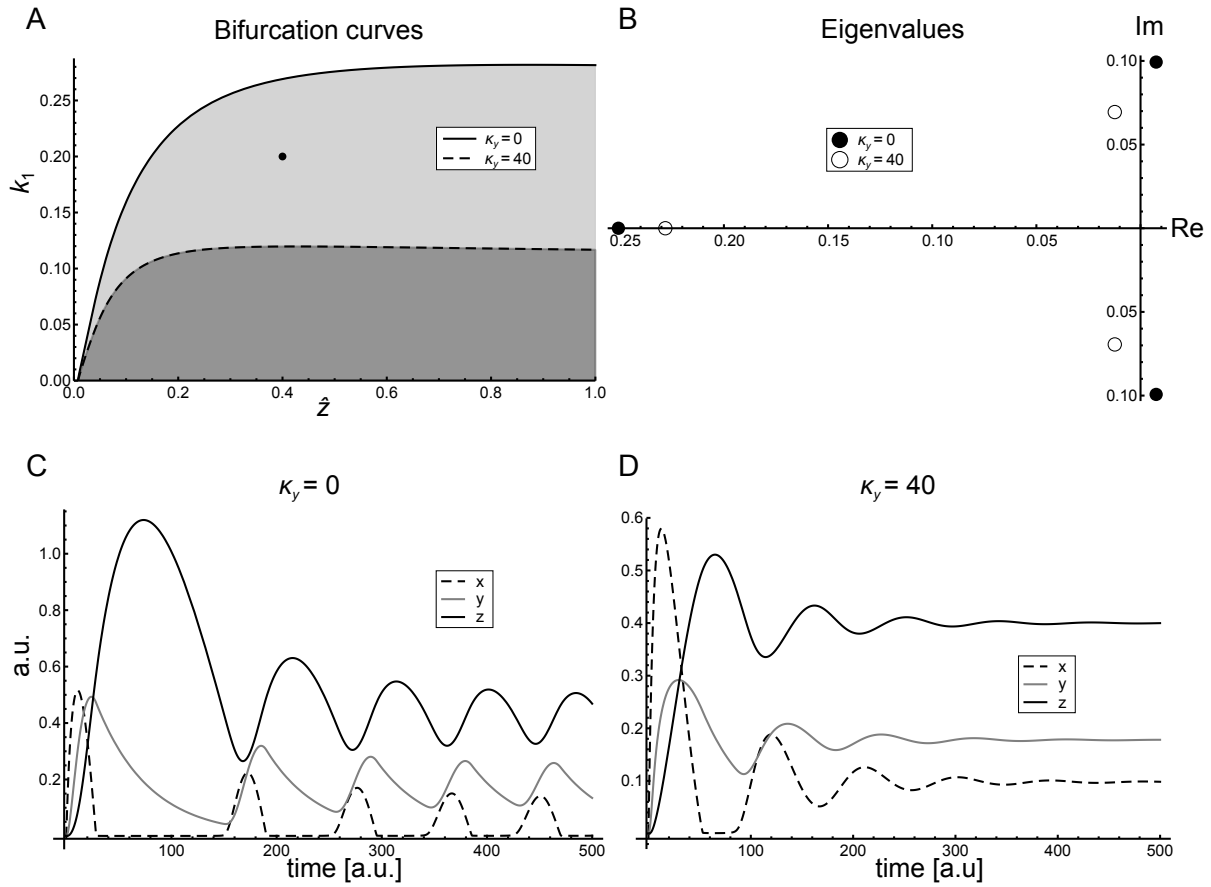

Figure S2 – Analysis of system (2.15) for $(\hat{z}, k_1) = (0.4, 0.2)$. **A**: Bifurcation curves $K_1(\hat{z}, \kappa_y)$. Shaded regions indicate where oscillations occur for $\kappa_y = 0$ (light gray) and $\kappa_y = 40$ (dark gray), respectively. The dot corresponds to $(\hat{z}, k_1)$. **B**: Eigenvalues of (2.10) for $\kappa = 0$ and $\kappa_y = 40$, respectively. **C**: Simulations of (2.15) for $\kappa_y = 0$. **D**: Simulations of (2.15) for $\kappa_y = 40$. Other parameters: $k_2 = 0.3$, $k_3 = k_5 = 0.1$, $k_4 = k_6 = 0.02$, $K_z = 0.05$, $K_x = 0.0001$, $m = 2$. For $\kappa_y = 40$, $\mu'(k_1^{crit}) = -0.21$ and the Lyapunov coefficient $l_1(k_1^{crit}) = -4777$. Thus, we have a subcritical Hopf bifurcation giving rise to stable limit cycles.

nary eigenvalues from the right half-plane into the left half-plane of $\mathbb{C}$ (Figure S2B).

In Figure S3 we demonstrate that assumption (2.6) is critical for the above analysis of the influence of κ_y on the stability of system (2.15). Note that for the parameters chosen for the simulation in Figure S3 $f_1(X(\hat{z}, 0)) \approx f_1(X(\hat{z}, 40)) < 0.97$, and thus just two percent less than in Figure S2. Figure S3 demonstrates that increasing κ_y does not necessarily eradicates oscillatory behaviour, when $f_1'(X(\hat{z}, \kappa_y)) \neq 0$. In the present case even the contrary happens, i.e. oscillation arise with increasing κ_y.

2.1.2 Example 2: Inflow-inhibition model with auto-inhibition in the y-component

For illustrating the role of auto-inhibitory feedbacks for the Goodwin-type models with signalling components, we set $q(z) = 1/(1 + K\, z^h)$ and $k_2 = 0$. Together with the other specifications from system (2.15)

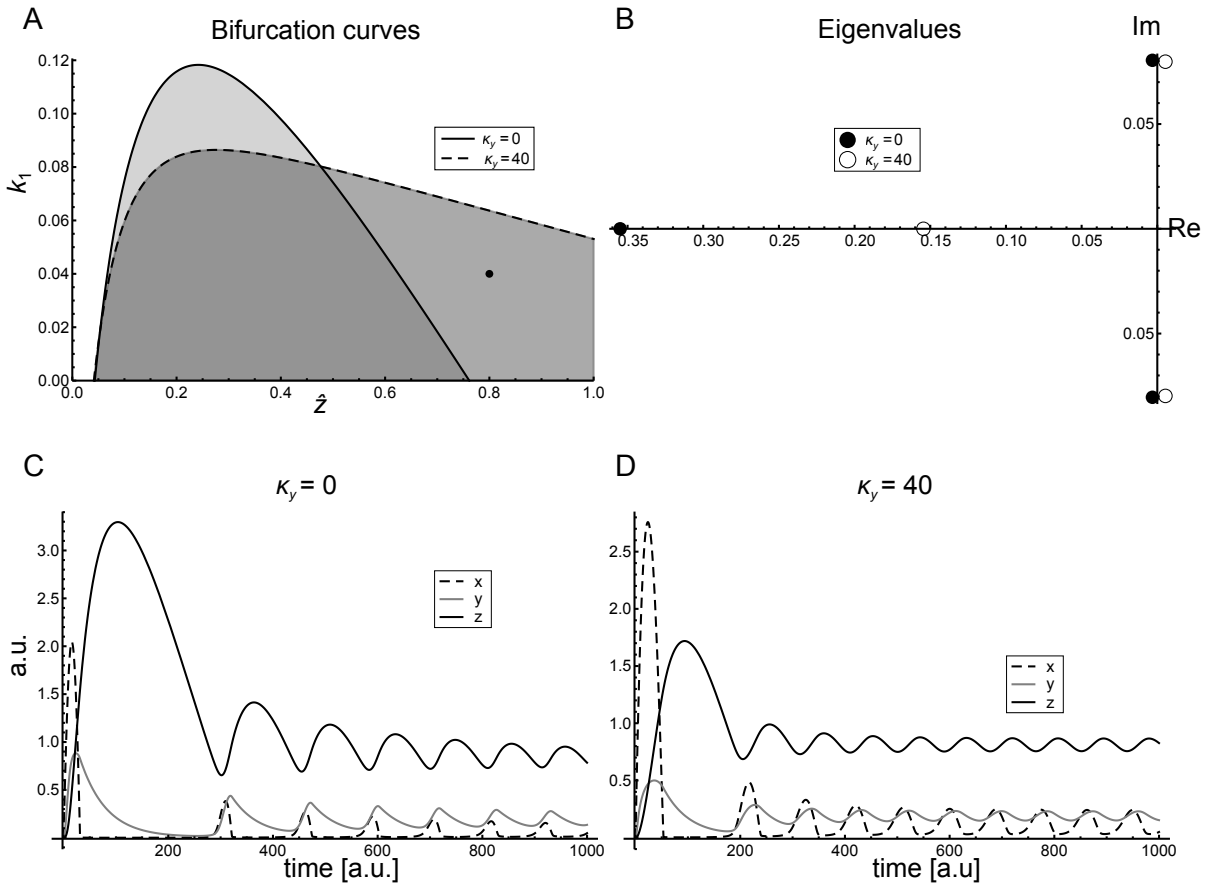

Figure S3 – Analysis of system (2.15) for $(\hat{z}, k_1) = (0.8, 0.04)$. **A**: Bifurcation curves $K_1(\hat{z}, \kappa_y)$. Shaded regions indicate where oscillations occur for $\kappa_y = 0$ (light gray) and $\kappa_y = 40$ (dark gray), respectively. The dot corresponds to $(\hat{z}, k_1)$. **B**: Eigenvalues of (2.10) for $\kappa_y = 0$ and $\kappa_y = 40$, respectively. **C**: Simulations of (2.15) for $\kappa_y = 0$. **D**: Simulations of (2.15) for $\kappa_y = 40$. Other parameters: $k_2 = 0.3$, $k_3 = k_5 = 0.1$, $k_4 = k_6 = 0.02$, $K_z = 0.05$, $K_x = 0.003$, $m = 2$. For $\kappa_y = 40$, $\mu'(k_1^{crit}) = -0.219$ and the Lyapunov coefficient $l_1(k_1^{crit}) = -215839$. Thus, we have a subcritical Hopf bifurcation giving rise to stable limit cycles.

we now have

$$\begin{aligned} \frac{dx}{dt} &= \frac{k_0}{1 + K\, z^h} - k_1\, x \\ \frac{dy}{dt} &= \frac{k_3\, x\, (y_T - y)}{1 + \kappa_y\, y^m} - k_4\, y \\ \frac{dz}{dt} &= k_5\, y - \frac{k_6\, z}{K_z + z}\ . \end{aligned} \tag{2.16}$$

The corresponding wiring scheme of the system (2.16) is represented in Figure S1B.

In Figure S4A we display the curve $K_1(\hat{z}, \kappa_y)$ according to (2.12) with (2.8) and (2.9) for $\kappa_y = 0$ and $\kappa_y = 10$, respectively. The dot in Figure S4A indicates a chosen $\hat{z}$ and k_1, for which the corresponding eigenvalues of (2.10) are displayed in Figure S4B for $\kappa_y = 0$ and $\kappa_y = 10$, respectively. Figures S4C and S4D display simulations of (2.16) for the chosen $\hat{z}$ and k_1 and for $\kappa_y = 0$ and $\kappa_y = 10$, respectively. For

the other parameter settings refer to the legend in Figure S4.

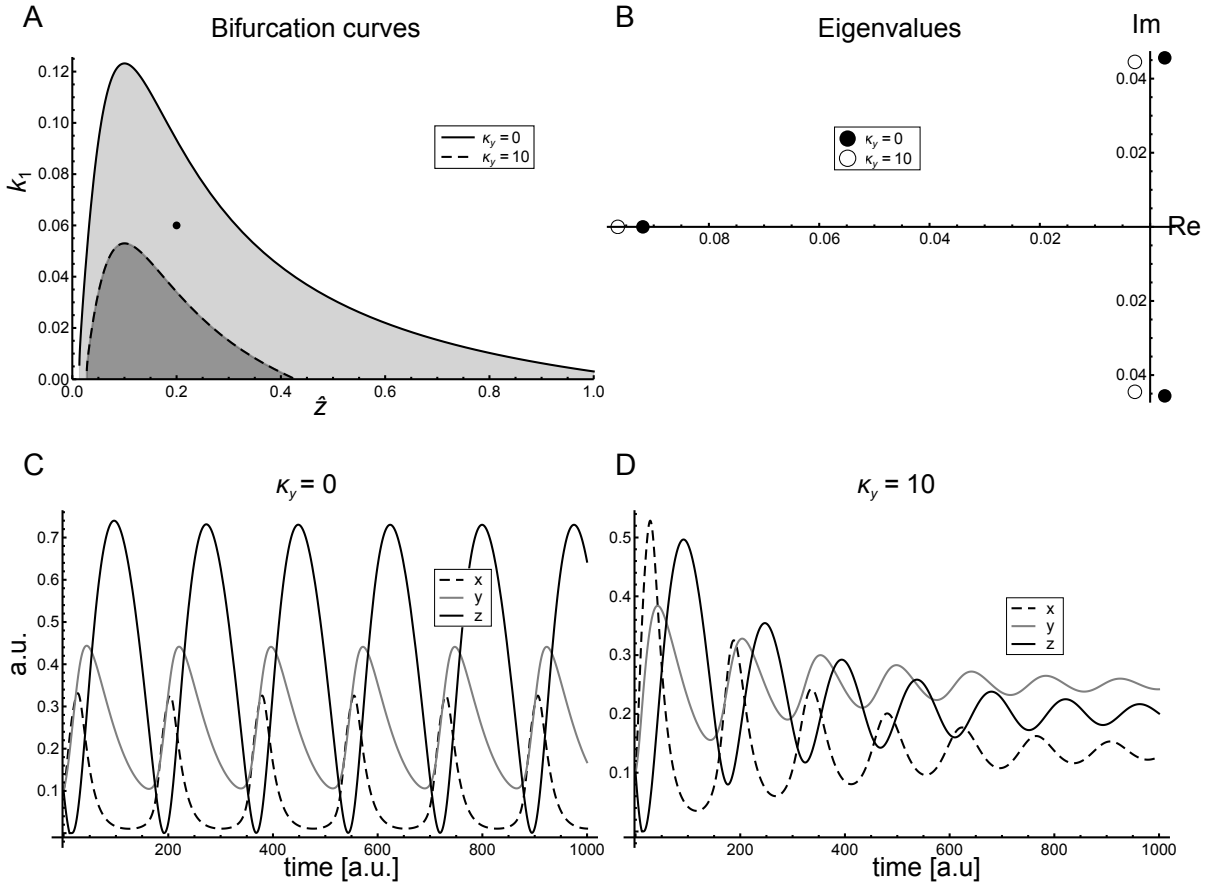

Figure S4 – Analysis of system (2.16) for $(\hat{z}, k_1) = (0.2, 0.06)$. **A**: Bifurcation curves $K_1(\hat{z}, \kappa_y)$. Shaded regions indicate where oscillations occur for $\kappa_y = 0$ (light gray) and $\kappa_y = 10$ (dark gray), respectively. The dot corresponds to $(\hat{z}, k_1)$. **B**: Eigenvalues of (2.10) for $\kappa_y = 0$ and $\kappa_y = 10$, respectively. **C**: Simulations of (2.16) for $\kappa_y = 0$. **D**: Simulations of (2.16) for $\kappa_y = 10$. Other parameters: $K = 100$, $h = 2$, $k_3 = k_5 = 0.08$, $k_4 = k_6 = 0.02$, $K_z = 1e^{-5}$, $m = 2$. For $\kappa_y = 10$,$\mu'(k_1^{crit}) = -0.32$ and the Lyapunov coefficient $l_1(K_1(\hat{z})) = -197860$. Thus, we have a subcritical Hopf bifurcation giving rise to stable limit cycles.

Figure S4 shows that, according to the subcritical Hopf bifurcation, the area below the curve $K_1(\hat{z}, \kappa_y)$ is the region, where the system oscillates. Figure S4A also clearly demonstrates that increasing κ_y decreases this region. Thus, for given values of $\hat{z}$ and k_1, we can increase κ_y such that the initially oscillating system (Figure S4C) is stabilised (Figure S4D), corresponding to a shift of the single pair of pure imaginary eigenvalues from the right half-plane into the left half-plane of $\mathbb{C}$ (Figure S4B). Notably, for the Goodwin-type models no restrictions as (2.6) apply, i.e. the oscillatory regions in always decreased for increasing κ_y.

Note that the cooperativity of the delayed feedback function $q(z) = 1/(1 + K\, z^h)$ is $h = 2$ in our case. This is well below the reported necessary cooperativity of 8 to get oscillations [2].

2.2 The κ_z-dependence of the bifurcation curve $K_1(\hat{z})$

We consider (1.1) with (2.1), where $H(z,\kappa_z)$ is of the form (2.2b), $g \equiv 1$, and $F(x,z) = f_1(x)\, f_3(z)$ with f_1 satisfying (2.6). Thus system (1.1) becomes

$$\begin{aligned} \frac{dx}{dt} &= k_0\, q(z) - \Big(k_1\, x + k_2\, f_1(x)\, f_3(z)\Big)\,, \\ \frac{dy}{dt} &= k_3\, x\, (y_T - y) - k_4\, y\,, \\ \frac{dz}{dt} &= k_5\, y\, H(z,\kappa_y) - k_6\, h(z)\,. \end{aligned} \tag{2.17}$$

In this case, the equilibrium functions (1.3) read

$$\hat{y} = Y(\hat{z},\kappa_z) := \frac{k_6\, h(\hat{z})}{k_5\, H(\hat{z},\kappa_z)} \le y_T\,, \quad \hat{x} = X(\hat{z},\kappa_z) := \frac{k_4\, Y(\hat{z},\kappa_z)}{k_3\,\big(y_T - Y(\hat{z},\kappa_z)\big)} \tag{2.18}$$

for the parameter value

$$\hat{k}_0 = P(k_1,\hat{z},\kappa_z) := \frac{1}{q(\hat{z})}\,\Big(k_1\, X(\hat{z},\kappa_z) + k_2\, f_3(\hat{z})\Big)\,. \tag{2.19}$$

With (2.6) the Jacobian of (2.17) at the steady state $\hat{E}(\hat{z})$ is given by

$$\begin{aligned} J(k_1,\kappa_z) &= \begin{bmatrix} -k_1 & 0 & -B(k_1,\hat{z},\kappa_z) \\ C(\hat{z},\kappa_z) & -D(\hat{z}) & 0 \\ 0 & E(\hat{z},\kappa_z) & -F(\hat{z},\kappa_z) \end{bmatrix} \\ &:= \begin{bmatrix} -k_1 & 0 & -(k_1\, B_1(\hat{z},\kappa_z) + B_0(\hat{z})) \\ k_3(y_T - Y(\hat{z},\kappa_z)) & -(k_4 + k_3\, X(\hat{z})) & 0 \\ 0 & k_5\, H(\hat{z},\kappa_z) & -[k_6\, h'(\hat{z}) + k_5\, Y(\hat{z})\, |H'(\hat{z},\kappa_z)|] \end{bmatrix} \\ &= \begin{bmatrix} -k_1 & 0 & -(k_1\, B_1(\hat{z},\kappa_z) + B_0(\hat{z})) \\ k_3(y_T - Y(\hat{z},\kappa_z)) & -(k_4 + k_3\, X(\hat{z})) & 0 \\ 0 & k_5\, H(\hat{z},\kappa_z) & -k_6\left[h'(\hat{z}) + h(\hat{z})\,\frac{|H'(\hat{z},\kappa_z)|}{H(\hat{z},\kappa_z)}\right] \end{bmatrix}. \end{aligned} \tag{2.20}$$

where

$$\begin{aligned} B_0(\hat{z}) &= k_2\, f_3(\hat{z}))\frac{|q'(\hat{z})|}{q(\hat{z})} + k_2\, f_3'(\hat{z}) \quad \text{and} \\ B_1(\hat{z},\kappa_z) &= X(\hat{z},\kappa_z)\frac{|q'(\hat{z})|}{q(\hat{z})}\,, \end{aligned} \tag{2.21}$$

Thus, according to (1.7), the critical curve $k_1 = K_1(\hat{z},\kappa_z)$ becomes – for fixed κ_z – the unique positive solution of the quadratic equation

$$0 = k_1^2 + R_1(\hat{z},\kappa_z)\, k_1 - R_0(\hat{z},\kappa_z)\,. \tag{2.22}$$

Note that with (2.21) and (2.18) $B_1(\hat{z},\kappa_z)\, C(\hat{z},\kappa_z)\, E(\hat{z},\kappa_z) = k_4\, k_5\, H(\hat{z},\kappa_z)\frac{|q'(\hat{z})|}{q(\hat{z})}$, such that the coefficients of (2.22) become

$$\begin{aligned} R_1(\hat{z},\kappa_z) =& D(\hat{z}) + F(\hat{z},\kappa_z) - \frac{k_4\, k_5\, H(\hat{z},\kappa_z)}{D(\hat{z}) + F(\hat{z},\kappa_z)}\,\frac{|q'(\hat{z})|}{q(\hat{z})} \quad \text{and} \\ R_0(\hat{z},\kappa_z) =& \frac{B_0(\hat{z})\, C(\hat{z},\kappa_z)\, E(\hat{z},\kappa_z)}{D(\hat{z}) + F(\hat{z},\kappa_z)} - D(\hat{z})\, F(\hat{z},\kappa_z)\,, \end{aligned}$$

We are interested in the κ_z-dependence of the positive solutions $K_1(\hat{z},\kappa_z)$ of (2.22). Therefore, in the following, we will omit the $\hat{z}$-dependence in some instances for simplicity.

By (2.3) one has $|H'(\hat{z},\kappa_z)| = n\,\kappa_z\,\hat{z}^{n-1}H^2(\hat{z},\kappa_z)$ and, therefore,

$$\begin{aligned} C(\kappa_z) =& k_3(y_T - Y(\hat{z},\kappa_z)) = k_3\Big(y_T - \frac{k_6\,h(\hat{z})}{k_5\,H(\hat{z},\kappa_z)}\Big)\,,\\ E(\kappa_z) =& k_5\,H(\hat{z},\kappa_z) \quad \text{and}\\ F(\kappa_z) =& k_6\left[h'(\hat{z}) + h(\hat{z})\,n\,\kappa_z\,\hat{z}^{n-1}H(\hat{z},\kappa_z)\right]\,. \end{aligned}$$

Thus, the κ_z-derivatives are given by

$$\begin{aligned} C'(\kappa_z) &= -\frac{k_3\,k_6\,h(\hat{z})\,\hat{z}^n}{k_5} \;<\; 0 \text{ and}\\ E'(\kappa_z) &= -k_5\,\hat{z}^n\,H^2(\hat{z},\kappa_z) \;<\; 0 \text{ and}\\ F'(\kappa_z) &= k_6\,h(\hat{z})\,n\,\hat{z}^{n-1}\,H^2(\hat{z},\kappa_z) \;>\; 0\;. \end{aligned} \tag{2.23}$$

implying

$$\begin{aligned} R_1'(\kappa_z) &= F'(\kappa_z) - \frac{k_4\,k_5}{(D+F(\kappa_z))^2}\frac{|q'|}{q}\Big(\frac{\partial}{\partial\kappa_z}H(\kappa_z)\,(D+F(\kappa_z)) - H(\kappa_z)F'(\kappa_z)\Big) \;>\; 0 \text{ and}\\ R_0'(\kappa_z) &= \frac{B_0\big(C'(\kappa_z)\,E(\kappa_z) + C(\kappa_z)E'(\kappa_z)\big)}{D+F(\kappa_z)} - \frac{B_0\,C(\kappa_z)\,E(\kappa_z)F'(\kappa_z)}{(D+F(\kappa_z))^2} - D\,F'(\kappa_z) \;<\; 0\;. \end{aligned} \tag{2.24}$$

Under $R_0(\kappa_z) > 0$, the positive zero $k_1 = K_1(\hat{z},\kappa_z)$ of (2.22) satisfies

$$\Big(2K_1(\hat{z},\kappa_z) + R_1(\hat{z},\kappa_z)\Big)\,\frac{\partial}{\partial\kappa_z}K_1(\hat{z},\kappa_z) \;=\; R_0'(\hat{z},\kappa_z) - K_1(\hat{z},\kappa_z)\,R_1'(\hat{z},\kappa_z) \tag{2.25}$$

together with (2.24) leading to

$$\frac{\partial}{\partial\kappa_z}K_1(\hat{z},\kappa_z) \;<\; 0 \tag{2.26}$$

and thus to a shrinking oscillation region in the $(\hat{z},k_1)$-plane for increasing κ_z. The oscillation region in the $(\hat{z},k_1)$-plane is the one below the graph of $k_1 = K_1(\hat{z},\kappa_z)$.

2.2.1 Example 3: Outflow-activation model with auto-inhibition in the z-component

For illustration, we set $f_1(x) = 1/(K_x + x)$, $f_3(z) = z$ and $h(z) = z/(K_z + z)$. Together with the above introduced specifications (2.1), with $H(z,\kappa_z) = 1/(1+\kappa_z\,z^n)$, and $g \equiv 1$, our system (1.1) becomes

$$\begin{aligned} \frac{dx}{dt} &= k_0 \;-\Big(k_1\,x + \frac{k_2\,x\,z}{K_x + x}\Big)\\ \frac{dy}{dt} &= k_3\,x\,(y_T - y) - k_4\,y\\ \frac{dz}{dt} &= \frac{k_5\,y}{1+\kappa_z\,z^n} - \frac{k_6\,z}{K_z + z}\;. \end{aligned} \tag{2.27}$$

The corresponding wiring scheme of the system (2.27) is represented in Figure S1C.

In Figure S5A we display the curve $K_1(\hat{z},\kappa_z)$ according to (2.18) and (2.22) for $\kappa_z = 0$ and $\kappa_z = 4$, respectively. The dot in Figure S5A indicates a chosen $\hat{z}$ and k_1 for which the corresponding eigenvalues

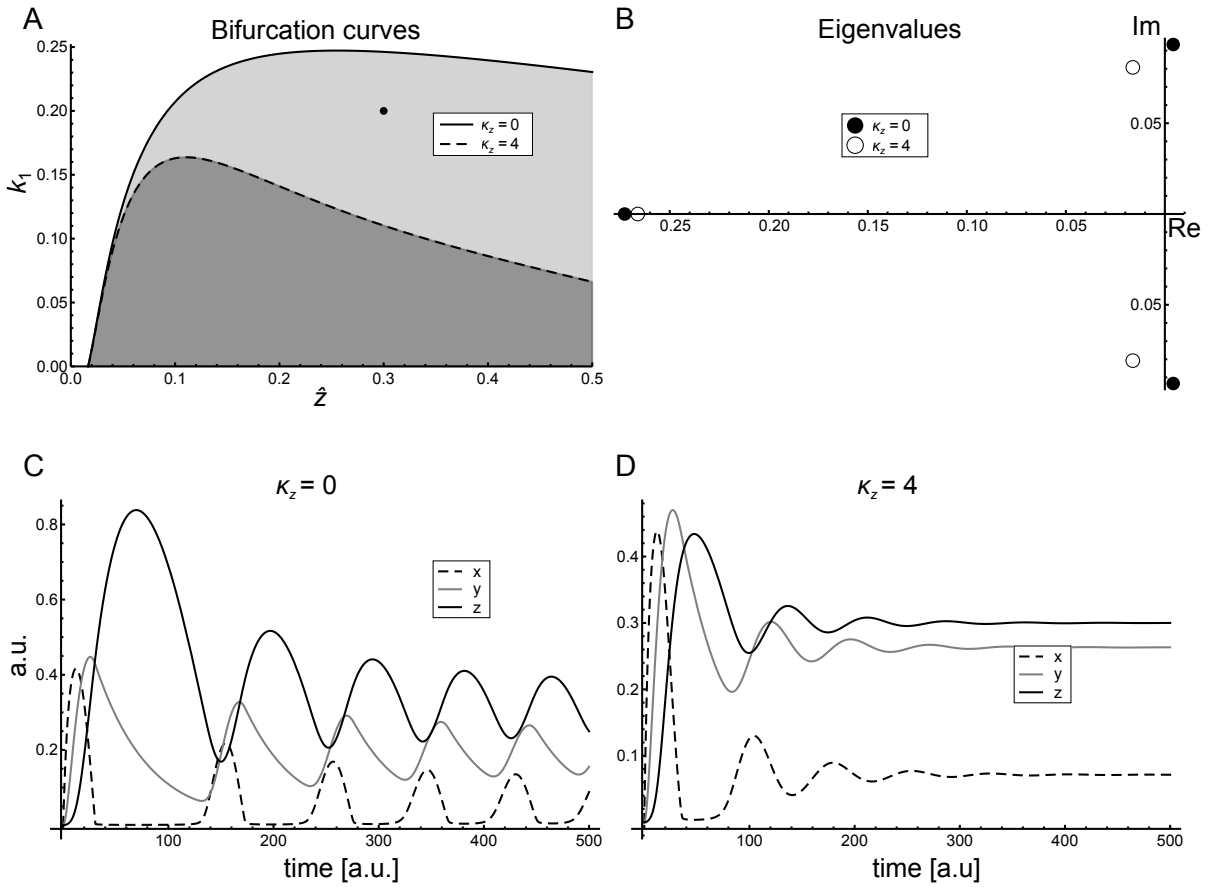

Figure S5 – Analysis of system (2.27) for $(\hat{z}, k_1) = (0.3, 0.2)$. **A**: Bifurcation curves $K_1(\hat{z}, \kappa_z)$. Shaded regions indicate where oscillations occur for $\kappa_z = 0$ (light gray) and $\kappa_z = 4$ (dark gray), respectively. The dot corresponds to $(\hat{z}, k_1)$. **B**: Eigenvalues of (2.20) for $\kappa_z = 0$ and $\kappa_z = 4$, respectively. **C**: Simulations of (2.27) for $\kappa_z = 0$. **D**: Simulations of (2.27) for $\kappa_z = 4$. Other parameters: $k_2 = 0.3$, $k_3 = k_5 = 0.1$, $k_4 = k_6 = 0.02$, $K_z = 0.01$, $K_x = 0.001$, $m = 2$. For $\kappa_z = 4$, $\mu'(k_1^{crit}) = -0.22$ and the Lyapunov coefficient $l_1(k_1^{crit}) = -25604$. Thus, we have a subcritical Hopf bifurcation giving rise to stable limit cycles.

of (2.20) are displayed in Figure S5B for $\kappa_z = 0$ and $\kappa_z = 4$, respectively. Figures S5C and S5D display simulations of (2.27) for the choosen $\hat{z}$ and k_1 and for $\kappa_z = 0$ and $\kappa_z = 4$, respectively. For the other parameter settings refer to the legend in Figure S5.

Figure S5 shows that, according to the subcritical Hopf bifurcation, the area below the curve $K_1(\hat{z}, \kappa_z)$ is the region, where the system oscillates. Figure S5A also clearly demonstrates that an increase of κ_z decreases this region. Thus, for given values of $\hat{z}$ and k_1, we can increase κ_z such that the initially oscillating system (Figure S5C) is stabilised (Figure S5D), corresponding to a shift of the single pair of pure imaginary eigenvalues from the right half-plane into the left half-plane (Figure S5B).

In Figure S6 we demonstrate that assumption (2.6) in this case is not as critical for the above analysis of the influence of κ_z on the stability of the system (2.27) as for (2.16). Note that, for the parameters chosen for the simulation in Figure S6, $f_1(X(\hat{z}, 0)) \approx f_1(X(\hat{z}, 4)) < 0.87$, i.e. much less than in Figure S3. In this case, increasing κ_z still decreases the oscillatory region, even though assumption (2.6) is somewhat

relaxed.

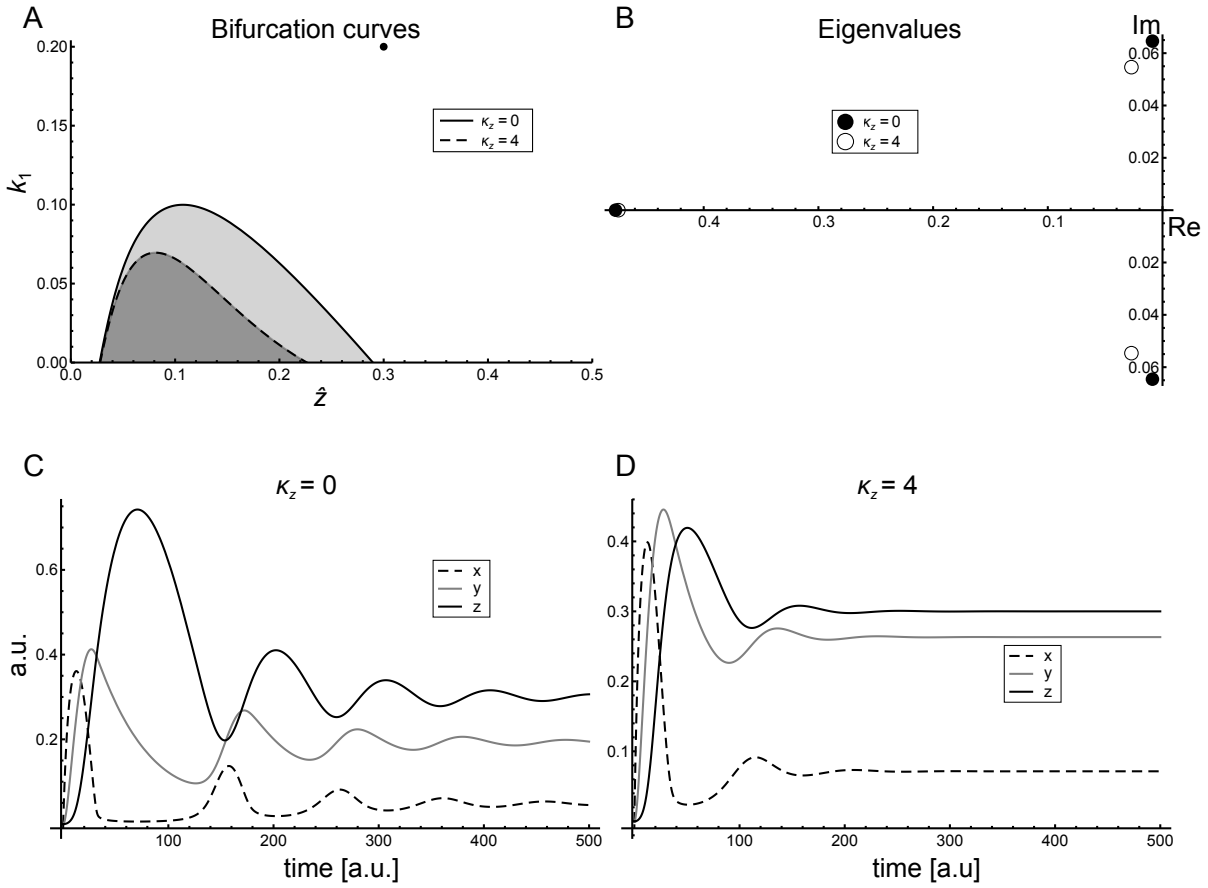

Figure S6 – Analysis of system (2.27) for $(\hat{z}, k_1) = (0.3, 0.2)$. **A**: Bifurcation curves $K_1(\hat{z}, \kappa_z)$. Shaded regions indicate where oscillations occur for $\kappa_z = 0$ (light gray) and $\kappa_z = 4$ (dark gray), respectively. The dot corresponds to $(q\hat{z}, k_1)$. **B**: Eigenvalues of (2.20) for $\kappa_z = 0$ and $\kappa_z = 4$, respectively. **C**: Simulations of (2.27) $\kappa_z = 0$. **D**: Simulations of (2.27) for $\kappa_z = 4$. Other parameters: $k_2 = 0.3$, $k_3 = k_5 = 0.1$, $k_4 = k_6 = 0.02$, $K_z = 0.01$, $K_x = 0.01$, $m = 2$. For $\kappa_z = 4$, $\mu'(k_1^{crit}) = -0.23$ and the Lyapunov coefficient $l_1(k_1^{crit}) = -101897$. Thus, we have a subcritical Hopf bifurcation giving rise to stable limit cycles.

2.2.2 Example 4: Inflow-inhibition model with auto-inhibition in the z-component

For illustrating the role of auto-inhibitory feedbacks for the Goodwin-type models with signalling components, we set $q(z) = 1/(1 + K\, z^h)$ and $k_2 = 0$. Together with the other specifications from (2.2) our system (1.1) becomes

$$\begin{aligned} \frac{dx}{dt} &= \frac{k_0}{1 + K\, z^h} - k_1\, x \\ \frac{dy}{dt} &= k_3\, x\, (y_T - y) - k_4\, y \\ \frac{dz}{dt} &= \frac{k_5\, y}{1 + \kappa_z\, z^m} - \frac{k_6\, z}{K_z + z}\ . \end{aligned} \tag{2.28}$$

The corresponding wiring scheme of the system (2.28) is represented in Figure S1D.

In Figure S7A we display the curve $K_1(\hat{z}, \kappa)$ according to (2.9) and (2.12) for $\kappa_z = 0$ and $\kappa_z = 1$, respectively.

The dot in Figure S7A indicates a chosen $\hat{z}$ and k_1, for which the corresponding eigenvalues of (2.20) are displayed in Figure S7B for $\kappa_z = 0$ and $\kappa_z = 1$, respectively. Figures S7C and S7D display simulations of (2.28) for the chosen $\hat{z}$ and k_1 and for $\kappa_z = 0$ and $\kappa_z = 1$, respectively. For the other parameter settings refer to the legend in Figure S7.

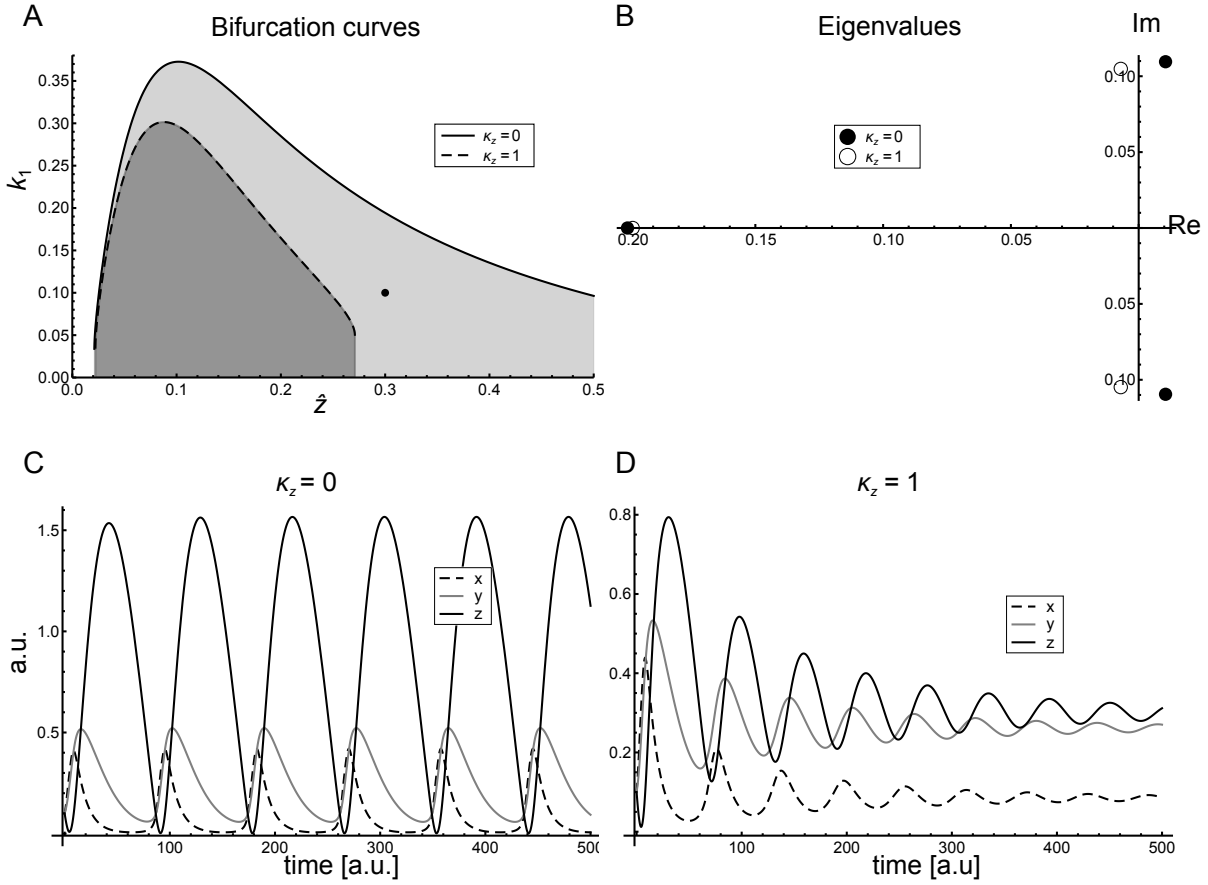

Figure S7 – Analysis of system (2.28) for $(\hat{z}, k_1) = (0.3, 0.1)$. **A**: Bifurcation curves $K_1(\hat{z}, \kappa_z)$. Shaded regions indicate where oscillations occur for $\kappa_z = 0$ (light gray) and $\kappa_z = 1$ (dark gray), respectively. The dot corresponds to $(\hat{z}, k_1)$. **B**: Eigenvalues of (2.20) for $\kappa_z = 0$ and $\kappa_z = 1$, respectively. **C**: Simulations of (2.28) for $\kappa_z = 0$. **D**: Simulations of (2.28) for $\kappa_z = 10$. Other parameters: $K = 100$, $h = 2$, $k_3 = k_5 = 0.25$, $k_4 = k_6 = 0.06$, $K_z = 0.0001$, $m = 2$. For $\kappa_z = 0$, $\mu'(k_1^{crit}) = -0.2$ and the Lyapunov coefficient $l_1(k_1^{crit}) = -1082$. Thus, we have a subcritical Hopf bifurcation giving rise to stable limit cycles.

Figure S7 shows that, according to the subcritical Hopf bifurcation, the area below the curve $K_1(\hat{z}, \kappa_z)$ is the region, where the system oscillates. Figure S7A also clearly demonstrates that increasing κ_z decreases this region. Thus, for given values of $\hat{z}$ and k_1, we can increase κ_z such that the initially oscillating system (Figure S7C) is stabilised (Figure S7D), corresponding to a shift of the single pair of pure imaginary eigenvalues from the right half-plane into the left half-plane of $\mathbb{C}$ (Figure S7B). Note that the cooperativity of the delayed feedback function $q(z) = 1/(1 + K\, z^n)$ is $n = 2$ in our case. This is well

below the reported necessary cooperativity of 8 in order to get oscillations [2].

3 The HOG system

3.1 The model

In order to describe the data provided in Figure 4 in the main text, we tested the following models based on our general framework (1.1):

$$\begin{aligned}\frac{dx}{dt} &= \frac{k_0 + NaCl}{(1 + K\, z^h)^{\delta_1}} - k_1\, x - (1-\delta_1)\frac{k_2\, x\, z}{(K_x + x)^{\delta_2}} \\ \frac{dy}{dt} &= \frac{k_3\, x(1-y)}{(1+\kappa\, y^n)^{\delta_3}} - k_4\, y \\ \frac{dz}{dt} &= k_5\, y - \frac{k_6\, z}{(K_z + z)^{\delta_4}}\ ,\end{aligned} \tag{3.1}$$

where $\delta = (\delta_1, \delta_2, \delta_3, \delta_4)$, $\delta_i \in \{0,1\}, i = 1, ..., 4$ indicate model alternatives. The model No. 6 with $\delta = (0,1,1,0)$ was selected the best approximating model (see Table 1 in the main text). Here, $x(t)$ is a putative sensor of the system reacting to the external stimulus $NaCl$, $y(t)$ represents phosphorylated Hog1, and $z(t)$ represents internal glycerol concentration. We further assumed a constant total concentration of phosphorylated and unphosphorylated Hog1 equivalent to 1.
From the data in Figure 4 is becomes clear that there is a non-zero steady state for the unperturbed situation ($NaCl = 0$) for phosphorylated Hog1 and internal glycerol, i.e. y_0 and z_0, respectively. Therefore, we arbitrarily set initial values for Hog1 and internal glycerol to $y_0 = 0.02$ and $z_0 = 0.2$ similar as in Schaber et al. (2012). In order to fit $x(t)$ and $z(t)$ to the data, we used the scaled variables $x_{scaled}(t) = 100\, x(t)/0.8$ and $z_{scaled}(t) = 17\, z(t)/z_0$, assuming that at maximum relative Hog1 phosphorylation, i.e. 80% of the total Hog1 are phosphorylated, and that the initial value of internal glycerol is 17% of its maximum after an osmotic shock of 0.5 $NaCl$ as in the data (see Figure 4C). The initial value x_0 of x was fitted to the data. The inhibition experiment (Figure 4B) was simulated by multiplying the simulated value of activated Hog1 by 0.001.
With the assumed, respectively fitted, initial concentrations, we reduced the number of free parameters by setting

$$\begin{aligned}k_0 &= \Big(k_1\, x_0 + \frac{k_2\, x_0\, z_0}{(K_x + x_0)^{\delta_2}}\Big) \quad \text{for} \quad \delta_1 = 0 \quad \text{and} \\ k_1 &= \frac{k_0}{x_0(1 + K\, z_0^h)} \quad \text{for} \quad \delta_1 = 1\end{aligned}$$

and

$$\begin{aligned}k_4 &= \frac{k_3\, x_0(1-y_0)}{y_0(1+\kappa\, y_0^n)^{\delta_3}} \\ k_6 &= \frac{k_5\, y_0\, (K_z + z_0)^{\delta_4}}{z_0}\ .\end{aligned}$$

Therefore, we are left with 8 free parameters that were fitted to the data. The estimated parameters of the best approximating model No. 6 (see Table 1 in the main text) are listed in Table SS2. The parametrised model and the data is provided in the Supplementary Material in COPASI format.

In Figure S8 the data and simulated values for model No. 2 ($\delta = (0,1,0,0)$) are displayed.

3.2 Bifurcation analysis

The best approximating model No. 6 with $\delta = (0,1,1,0)$ employed an auto-inhibition ($\delta_3 = 1$). However, the corresponding model without auto-inhibition, i.e. model No. 2 with $\delta = (0,1,0,0)$ (ranked third, Table 1 in the main text) performed almost equally as good with respect to the AIC (see Table 1, main

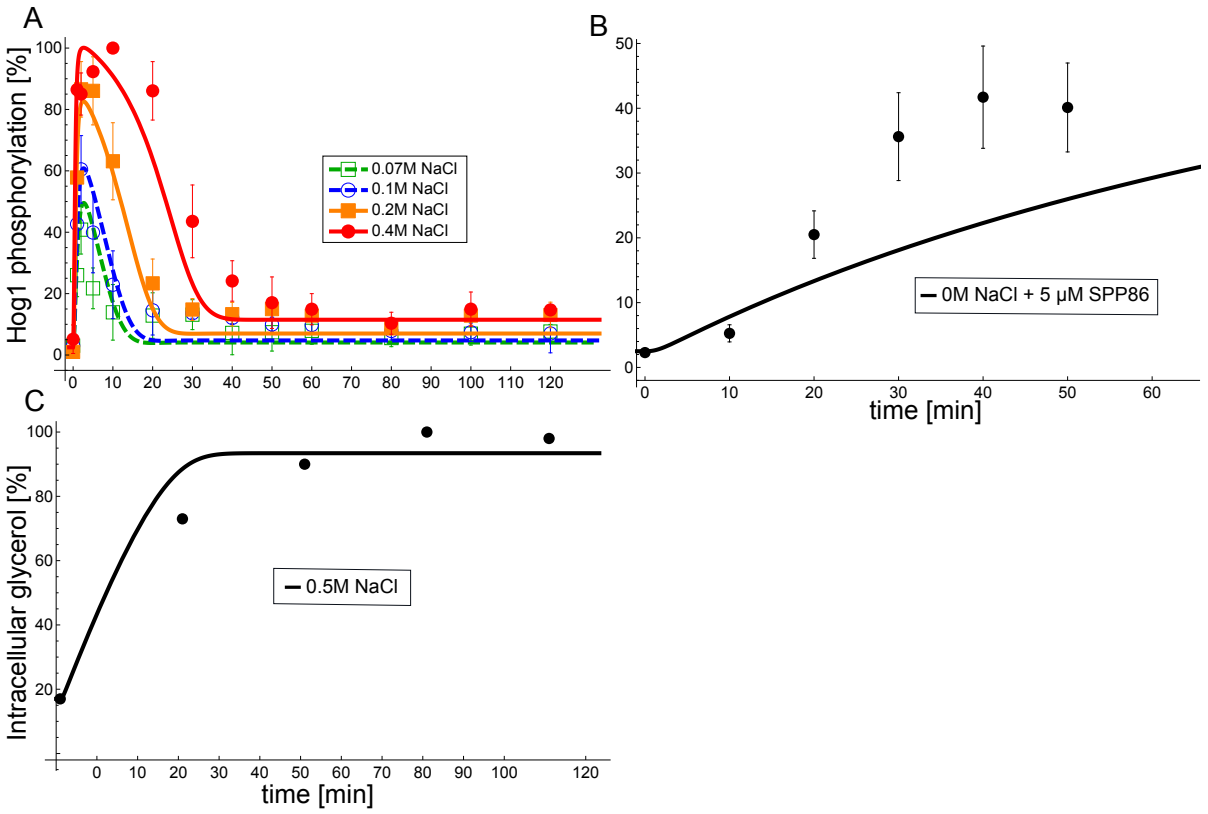

Figure S8 – HOG system. Data and fit for the model No. 2 ($\delta = (0, 1, 0, 0)$). **A**: Measured (dots) and simulated (lines) phosphorylated Hog1 (y) for different osmotic stress conditions. **B**: Measured (dots) and simulated (lines) phosphorylated Hog1 (y) in an experiments without osmotic shock and where Hog1 kinase activity was inhibited by the kinase inhibitor SPP86. **C**: Measured (dots) and simulated (lines) glycerol (z) upon an osmotic shock of 0.5M NaCl.

text) and had similar parameter values. Therefore, we compared the stability of the steady states of the two models for an osmotic shock of 0.5M NaCl with respect to different parameter combinations. The glycerol production parameter k_5 was the most sensitive with respect to steady state stability, therefore, we plotted the steady state stability in two dimensions, where the horizontal axis corresponds to k_5 and the vertical axis to other estimated parameters and initial conditions, respectively (Figure 5 and Figure S9).

The permissive region where oscillations occur in the respective two-dimensional parameter space is always smaller for the model with auto-inhibition (model No. 6, dark gray regions) compared to the model without auto-inhibition (model No. 2, light gray regions).

3.3 Monte Carlo analysis of steady state sensitivities

In models of biological systems constant parameters are usually simplifications of underlying biochemical processes, which are assumed to be constant in the actual setting. As this assumption usually only holds approximately, it is of interest to consider properties of the system under small parameter perturbations.

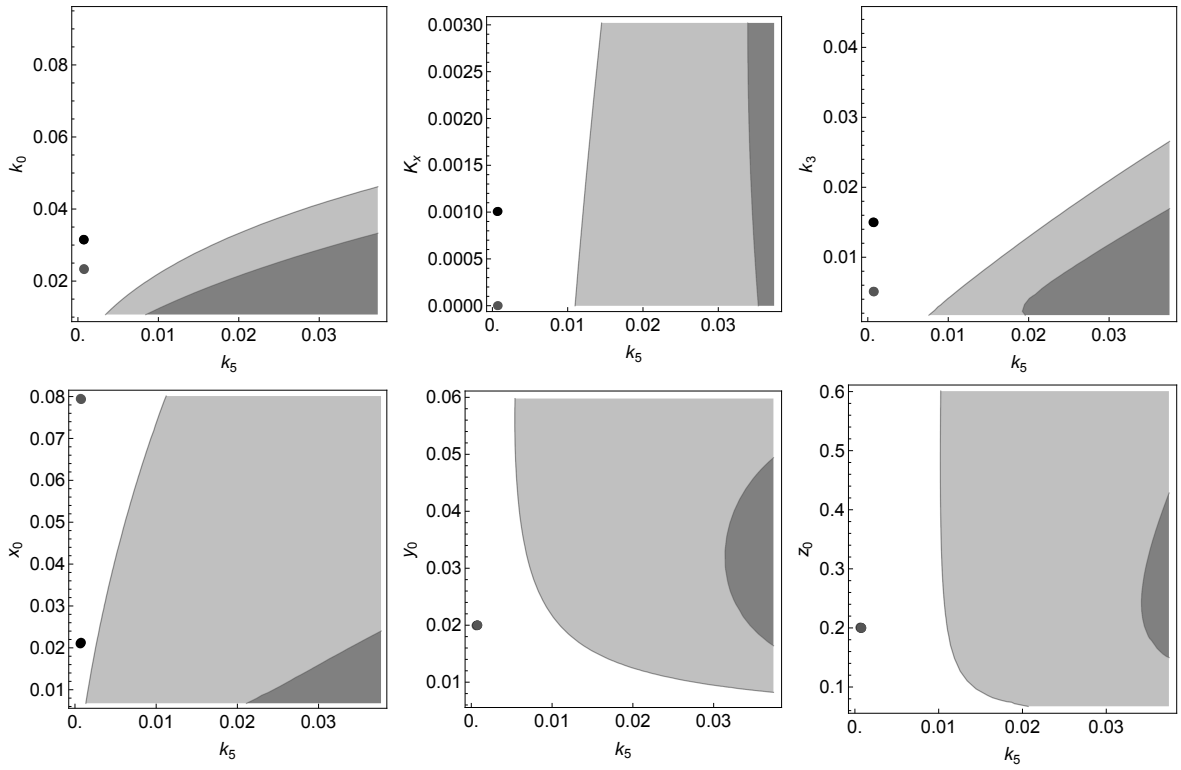

Figure S9 – Stability and bifurcation analysis. Gray and light gray indicate regions with unstable steady state, i.e. where oscillations occur, for the system with (Model No. 6) and without feedback (Model No. 2), respectively. Black and dark gray dots indicate the fitted parameters for the system with (Model No. 6) and without feedback (Model No. 2), respectively. The boundary between white and shaded regions indicates bifurcation lines in the respective two-dimensional parameter space.

Here, we consider the equilibrium of the best approximating models with and without auto-inhibition, i.e. model No. 6 ($\delta = (0, 1, 1, 0)$) and model No. 2 ($\delta = (0, 1, 0, 0)$, ranked third, Table 1 in the main text), respectively, in order to investigate, whether the auto-inhibitory feedback in the HOG model system stabilizes the steady state after adaptation. To this end, we performed a Monte Carlo analysis. All free parameters of the best approximating model No. 6 and the according model without auto-inhibitory feedback (Model No. 2) were simultaneously perturbed by sampling the respective parameter 1000 times from a uniform distribution ranging from half to double of its original value. Subsequently, we calculated the according steady states after an osmotic shock on 0.2 M $NaCl$. In Table SS1 we list some test statistics concerning differences in location (U test, K-S test,) and scale (S-T test, C test) concerning the resulting distributions of the difference between the original steady state and the perturbed steady state. The steady states of $\hat{x}$ and $\hat{y}$ were significantly less sensitive to parameter perturbations in the model with auto-inhibition.

Table S1 – HOG model Monte Carlo analysis. Variance measures and test statistics.

	$\hat{x}$		$\hat{y}$		$\hat{z}$	
Model	w/o FB	with FB	w/o FB	with FB	w/o FB	with FB
Variance	0.02	0.005	0.001	0.001	0.025	0.026
IQR	0.17	0.06	0.04	0.04	0.21	0.21
U test		-		-		-
K-S test		***		-		-
S-T test		***		-		-
C test		***		**		-

w/o: without, IQR: Interquartile range, U: Mann-Withney, K-S: Kolmogoroff-Smirnov, S-T: Siegel-Tukey, C: Conover,***: $P < 0.01$, **: $P < 0.05$, *: $P < 0.1$, -:$P > 0.1$, where P is the P-value of the respective test.

4 The p53 system

4.1 The model

In order to describe the data provided in Figure 7 in the main text, we tested the following models based on our general framework (1.1):

$$\begin{aligned}\frac{dx}{dt} &= \frac{k_0}{(1+K\,z^h)^{\delta_1}} - k_1\,x - (1-\delta_1)\frac{k_2\,x}{(K_x+x)^{\delta_2}}\,\frac{z^{n\,\delta_3}}{(K_1^n+z^n)^{\delta_3}}\\ \frac{dy}{dt} &= k_3\,x - k_4\,y\\ \frac{dz}{dt} &= \frac{k_5\,y}{(1+\kappa z^m)^{\delta_4}} - \frac{k_6\,z}{(K_z+z)^{\delta_5}}\ ,\end{aligned} \tag{4.1}$$

where $\delta = (\delta_1, \delta_2, \delta_3, \delta_4, \delta_5)$, $\delta_i \in \{0, 1\}, i = 1, ..., 5$ indicate model alternatives. The model No. 11 with $\delta = (0, 0, 1, 0, 1)$ was selected as the best approximating model (see Table 3 in the main text). Here, $x(t)$ is activated p53 and the transducer $y(t)$ is an intermediate component, e.g. Mdm2 RNA. Consequently, for the latter component no mass conservation is assumed. The response $z(t)$ is Mdm2 protein concentration, which in turn mediates p53 degradation.
Opposed to the HOG system, the data indicated initial concentrations of p53 and Mdm2 of zero. Therefore, we set the initial concentrations of all variables to zero. This impeded reducing the dimensionality of the parameter estimation problem as for the HOG system. Thus, we estimated all model parameters. The estimated parameters of the best approximating model No. 11 (see Table 3 in the main text) are listed in Table SS3. COPASI was unable to calculate asymptotic confidence intervals because of the singularity of the Fisher information matrix. The parametrised model No. 11 is provided in the Supplementary Material in COPASI format.

4.2 Bifurcation analysis

As for the HOG model, we conducted a bifurcation analysis for the best approximating model No. 11 ($\delta = (0, 0, 1, 0, 1)$) by analysing the stability of steady states with respect to different parameter combinations (Figure S10). In this case, the best approximating model employed no auto-inhibition, i.e. $\delta_4 = 0$. However, the corresponding model with auto-inhibition, i.e. model No. 15 ($\delta = (0, 0, 1, 1, 1)$), which was ranked second (see Table 3 in the main text), showed rather different stability regions, and, therefore, we

Table S2 – Estimated free parameters of the best approximating HOG model No. 6 ($\delta = (0, 1, 1, 0)$) with estimated asymptotic standard deviation (stdev)

parameter	value	stdev
x_0	0.0212649	0.0580806
k_1	0.0314835	0.0856927
k_2	0.53387	0.0217899
K_x	0.00100833	0.00296022
κ_y	5.93877	0.109613
h	1	0.109613
k_3	0.0149781	0.00620738
k_5	0.000752464	5.56738e-05

Table S3 – Estimated free parameters of the best approximating p53 model No. 11 ($\delta = (0, 0, 1, 0, 1)$)

parameter	value
k_0	0.234571
k_1	2.78481e-06
k_2	2.16401
K_1	0.644017
n	9.42914
k_3	2.33117
k_4	1.18023
k_5	0.570981
k_6	0.556487
K_z	0.0478507

refrained from a direct comparison of the two models. Instead, we analysed the stability of model No. 11 with and without auto-inhibtion by leaving all other parameters unchanged.

Not for all parameter sets a steady state existed, because $h(z) = z/(K_z+z)$ in (4.1) was limited. These parameter combinations are indicated by hashed areas in Figure S10. In Figure S10 all parameters of the model are used as bifurcaton parameter at least once. The unstable region decreases by introducing an auto-inhibitory negative feedback. Moreover, upon addition of the auto-inhibitory feedback, the stability of the system changes, moving it from an unstable fixed point with limit cycle oscillations to a stable fixed point.

4.3 Monte Carlo analysis of steady state sensitivities

As above, we considered the equilibrium of the best approximating model with and without feedback, i.e. model No. 15 and model No. 11, respectively, under simultaneous perturbation of all free parameters, in order to investigate, whether an auto-inhibitory feedback in the p53 model system stabilizes the steady state. To this end, we performed a Monte Carlo analysis. All free parameters of the best approximating model No. 11 and the according model with auto-inhibitory feedback (Model No. 15, ranked second, Table 3 in the main text) were simultaneously perturbed by sampling the respective parameter 1000 times from a uniform distribution ranging from half to double of its original value. Subsequently, we calculated the according steady states, if they existed. In Table SS4 we list some test statistics concerning differences in location (U test, K-S test,) and scale (S-T test, C test) concerning the resulting distributions of the difference between the original steady state and the perturbed steady state. For the model with auto-inhibition (model No. 15) all steady states were significantly less sensitive to parameter perturbations.

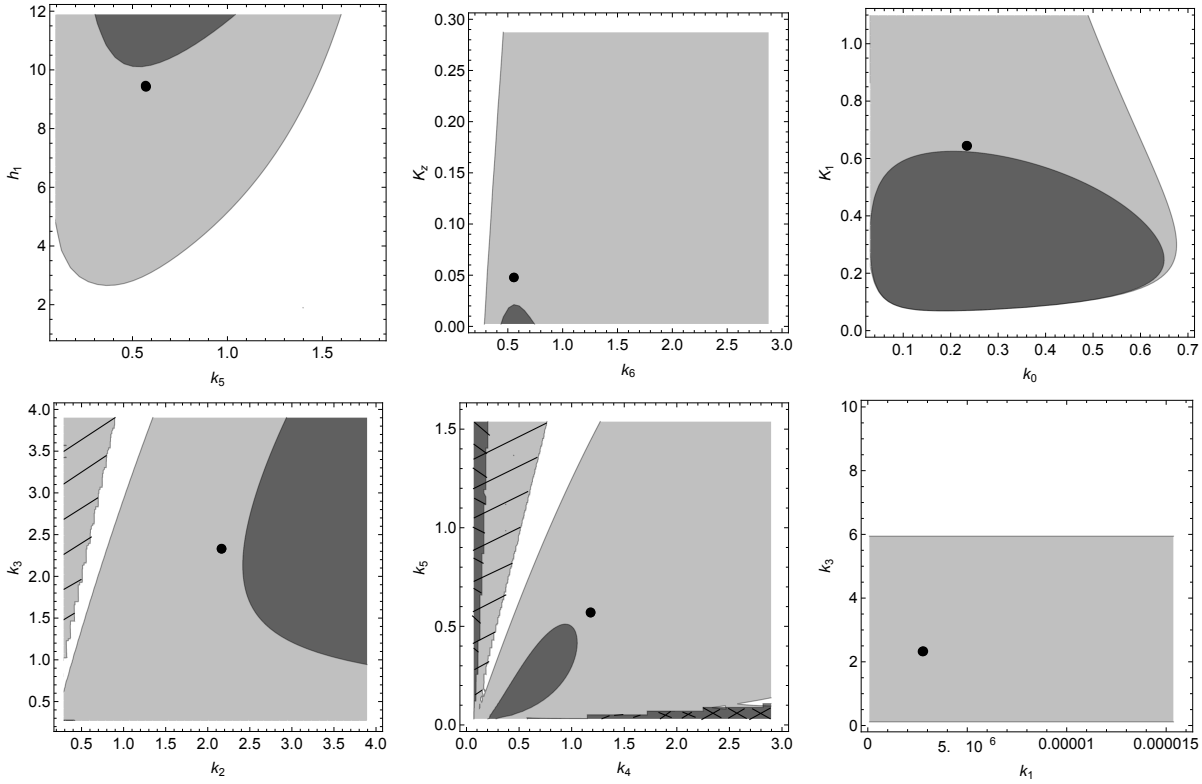

Figure S10 – Stability and bifurcation analysis for the best approximating model No. 15. Gray and light gray indicate regions with unstable steady state, i.e. where oscillations occur, for the system with ($\kappa = 1.25^3$, $h_2 = 3$) and without (original) feedback, respectively. The boundary between white and shaded regions indicates bifurcation lines in the respective two-dimensional parameter space. The hashed regions indicate parameter combinations which do not result in equilibria.

Table S4 – p53 model Monte Carlo analysis. Variance measures and test statistics.

	$\hat{x}$		$\hat{y}$		$\hat{z}$	
Model	w/o FB	with FB	w/o FB	with FB	w/o FB	with FB
Variance	0.28	0.24	1.74	0.32	0.1	0.09
IQR	0.52	0.49	1.55	0.65	0.48	0.44
U test	-		**		-	
K-S test	-		***		*	
S-T test	*		***		***	
C test	***		***		***	

w/o: without, IQR: Interquartile range, U: Mann-Withney, K-S: Kolmogoroff-Smirnov, S-T: Siegel-Tukey, C: Conover,***: $P < 0.01$, **: $P < 0.05$, *: $P < 0.1$, -:$P > 0.1$, where P is the P-value of the respective test.

References

1. Goodwin BC. Oscillatory behavior in enzymatic control processes. Adv Enzyme Regul. 1965;3:425–438.

2. Griffith JS. Mathematics of cellular control processes. I. Negative feedback to one gene. J Theor Biol. 1968 Aug;20(2):202–208.

3. Kuznetsov IUA. Elements of Applied Bifurcation Theory. Applied Mathematical Sciences. Springer, New York; 2004.